Chemical Geology 680 (2025) 122686

Contents lists available at ScienceDirect

Chemical Geology

journal homepage: www.elsevier.com/locate/chemgeo

Overcoming analytical limitations with 5-line multi-dynamic Nd isotope measurements by thermal ionisation mass spectrometry

C. Israel [a,*,1], C. Chauvel [a], T.-H. Luu [a], E.C. Inglis [a,2], D. Roberts [b]

[a] *Université Paris Cité, Institut de Physique du Globe de Paris, CNRS, 75005 Paris, France*
[b] *Nu Instruments Ltd, Unit 74, Clywedog Road South, Wrexham Industrial Estate, LL13 9XS, UK*

ARTICLE INFO

Editor: S Aulbach

Keywords:
TIMS
^{142}Nd
Multi-dynamic measurement
Nuclear field shift
High-precision
Sm interferences

ABSTRACT

The extinct ^{146}Sm—^{142}Nd radio-isotope chronometer is a valuable tool to study the first 500 Myr of Earth's history, although the entire range of variations of the ^{142}Nd/^{144}Nd ratio in terrestrial materials is on the order of 20 ppm only. The challenge is that measuring small isotope variations needs very high precision measurements (better than 5 ppm), which are difficult to obtain.

Here we present high-precision measurements of Nd isotope ratios performed over a period of three years using the latest generation Thermal Ionisation Mass Spectrometer (TIMS) developed by Nu Instruments – Nu TIMS. The Nu TIMS comprises 16 fixed Faraday cups and a zoom optics system that allow 5-line multi-dynamic analyses with the acquisition of three dynamic ratios for all Nd isotopes. This new method, coupled with an enhanced Nd^+ signal provides precise measurements with internal errors lower than 2 ppm on ^{142}Nd/^{144}Nd.

We assess the performance of the method using multiple measurements of JNdi-1 and AMES Rennes Nd pure standards, together with rock reference materials. For example, typical JNdi-1 measurements performed over a period of 19 months average at ^{142}Nd/^{144}Nd = 1.1418299 ± 36 (2sd – 3.2 ppm), ^{143}Nd/^{144}Nd = 0.5121007 ± 10 (2.0 ppm), ^{145}Nd/^{144}Nd = 0.3484046 ± 6 (1.8 ppm), ^{148}Nd/^{144}Nd = 0.2415790 ± 10 (4.1 ppm) and ^{150}Nd/^{144}Nd = 0.2364481 ± 27 (11.3 ppm). With such precision and accuracy, subtle variations of ^{142}Nd/^{144}Nd ratios, as low as 3 ppm, can now be detected in natural samples.

Minute differences in ^{145}Nd/^{144}Nd, ^{148}Nd/^{144}Nd and ^{150}Nd/^{144}Nd ratios can now also be detected in natural samples, allowing better identification of nucleosynthetic anomalies in extra-terrestrial samples. For terrestrial samples, it allows detection of traces of samarium, and of nuclear field shift effect due to analytical issues. In particular, we demonstrate that some Sm is present in the JNdi-1 standard and affects both its ^{148}Nd/^{144}Nd and ^{150}Nd/^{144}Nd ratios, making a systematic interference correction necessary. By detecting the existence of nuclear field shift effect on Nd isotopes, we can now prevent mis-interpretations of ^{142}Nd/^{144}Nd deviations that could be wrongly attributed to radiogenic signatures acquired during the Hadean.

1. Introduction

Radio-isotopes are valuable geochronometers and tracers, allowing elucidation of a wide range of geological and planetary processes. Neodymium, one of the Rare Earth Elements (REE), has seven isotopes, two of which are radiogenic. Samarium-147 decays slowly ($T_{1/2} = 106$ Ga) to ^{143}Nd and is widely used to study ancient geological processes. In contrast, the decay of ^{146}Sm ($T_{1/2} = 103$ Ma) produced ^{142}Nd during the first 500 Ma of Earth's history, and is now an extinct radionuclide. As such, variations in ^{142}Nd abundances can only result from changes in the Sm/Nd ratio during the very early part of Earth's history. Samarium and Nd are both highly refractory lithophile elements but Nd is slightly more incompatible than Sm, leading to its enrichment in melt products (e.g., the crust) compared to residual materials (e.g., the depleted mantle). The ^{147}Sm—^{143}Nd and ^{146}Sm—^{142}Nd systems have been widely used in the study of the oldest continental rocks dating back to ~4 Ga (e.g., Nuvvuagittuq, Canada, 3.8–4.3 Ga – O'Neil et al., 2008, 2011), providing robust insights into the evolution of the oldest accessible continents and early mantle depletion events. While variations in ^{142}Nd abundance in Archean samples are significant, most rocks formed later

---

* Corresponding author.
E-mail address: ci265@cam.ac.uk (C. Israel).
[1] Present address: Department of Earth Sciences, University of Cambridge, Downing Street, Cambridge CB2 3EQ, UK.
[2] Present address: School of Earth and Environmental Science, Main Building, Cardiff University, Cardiff, Wales, CF10 3AT.

https://doi.org/10.1016/j.chemgeo.2025.122686
Received 10 October 2024; Received in revised form 12 February 2025; Accepted 14 February 2025

show no clear isotopic variations relative to the contemporary terrestrial mantle (see Fig. 2 in O'Neil et al., 2024). In particular, ocean island basalts (OIB) generally show no pronounced variations (see Weis et al., 2023 for a compilation), although there are few exceptions. For example, Peters et al. (2018, 2021) and Horan et al. (2018) report small ^{142}Nd isotope anomalies in a few samples from Réunion and Samoa islands and interpret them as evidence for the involvement of Hadean material. Nevertheless, such evidences are rare and interpretations are limited by the reported analytical precision (~5 ppm reproducibility).

Over decades, advances in mass spectrometry have greatly improved the precision of isotope analysis, as demonstrated by the increased reproducibility on Sr and Nd radiogenic isotopes from tens of ppm thirty years ago to a few ppm today (e.g., Patchett and Ruiz, 1987; Luu et al., 2022). Measurements of ^{142}Nd/^{144}Nd ratios are usually done using Thermal Ionisation Mass Spectrometry (TIMS) because it usually offers superior precision over its Multi-Collector Inductively Coupled Plasma Mass Spectrometry (MC-ICP-MS) counterpart, owing to sustained beam stability and enhanced counting statistics acquired during prolonged analyses. In the 1990s, the first dynamic measurements of ^{142}Nd/^{144}Nd ratios achieved a reproducibility of 9 ppm on synthetic standards (Nyquist et al., 1991; Harper Jr and Jacobsen, 1992), value that dropped down to 5 ppm over the last decade using a 2-line dynamic method (Roth et al., 2014) or a 4-line multi-dynamic method (Garçon et al., 2018). Only few studies achieved a reproducibility down to 2.4 ppm (e.g., Caro et al., 2006; Hyung and Tissot, 2021). In parallel, recent developments on MC-ICP-MS have challenged TIMS measurements by using a different approach to counting statistics relying on multiple short static analyses of the same sample bracketed with standards to lower the error on ^{142}Nd/^{144}Nd ratios (e.g., Saji et al., 2016 report 2.4 ppm reproducibility on ^{142}Nd/^{144}Nd).

In this study, we present Nd isotope measurements obtained using the latest generation of TIMS developed by Nu Instruments (Wrexham, UK). Its 16 fixed Faraday cups coupled with an efficient zoom optics system enable simultaneous measurement of a wide mass range. For example, Luu et al. (2022) developed 5-line multi-dynamic methods to precisely measure ^{143}Nd/^{144}Nd and ^{87}Sr/^{86}Sr ratios. Here, we demonstrate that the 5-line method actually provides robust and high-precision analyses for all Nd isotopic ratios. Using this technique, we report isotopic measurements for a selection of international rock reference materials and highlight that accurate measurement of all Nd isotopes provides tools to identify analytical artefacts that may bias interpretations.

2. Analytical techniques

2.1. Materials

We selected two pure Nd standard solutions, with supposedly invariant mass-independent ^{142,145,148,150}Nd/^{144}Nd isotope ratios: the Geological Survey of Japan JNdi-1 standard provided as a Nd oxide powder and the AMES Rennes Nd standard prepared from pure Nd metal. Both standards were dissolved in 2.5 M HCl to give 800 μg/g Nd stock solutions.

In addition to the pure standards, we analysed six terrestrial rock reference materials from the United States Geological Survey (USGS) and the International Working Group (GIT-IWG). The USGS rock reference materials are basalts from Columbia River (BCR-2), Hawaii (BHVO-2) and Iceland (BIR-1), an andesite from Guano Valley (AGV-2) and a rhyolite from Glass Mountain (RGM-1). The GIT-IWG reference material is a basalt from an ancient French volcano near Nancy (BE-N).

2.2. Chemical procedure for the terrestrial rock reference materials

All samples in this study were processed in a clean room at the Institut de Physique du Globe de Paris (IPGP, France). One hundred to 360 mg of rock powders were acid-digested in Teflon beakers using a 3:1, 28 M HF/15 M HNO_3 mixture (2 ml of HF for 50 mg of rock powder) maintained at 75 °C on a hot plate for 48 h followed by evaporation to incipient dryness. A second digestion step with 6 M HCl was performed and followed by three cycles of dissolution using a 1:1, 15 M HNO_3/6 M HCl mixture and slow evaporation at 70 °C to remove the potential fluoride phases which may have formed during sample decomposition.

Neodymium was isolated using the four-step procedure described in Garçon et al. (2018) and detailed in Table 1. Rare Earth elements were first separated from the main matrix using AG50W-X8 cation exchange resin. Cerium was then isolated from the other REE using an LN resin and an oxidative technique that allows the tetravalent Ce to stick onto the resin while the trivalent REE are eluted, before being reduced and released. This step was completed twice to ensure a complete removal of Ce. The Ce-free REE fraction was then purified using AG50W-X8 resin to eliminate the Na and Br introduced in the previous step. Neodymium was finally isolated from Sm and HREE using a thin column filled with LN resin and the successive elution of LREE, Nd and HREE.

For each sample, a 5 % aliquot of the isolated Nd fraction was analysed for elemental concentrations at IPGP using an Agilent 8900 ICP-MS/MS. The recovery yield was always between 93 and 100 % for 1000 to 7000 ng of Nd loaded onto the columns, except for one BCR-2 fraction with 76 % recovery (Table 3). The procedure efficiently eliminates interfering elements such as Ce (Ce/Nd $<$ 0.1 ‰) and Sm (Sm/Nd $<$ 0.1 ‰), and limits the quantity of Pr (Pr/Nd $<$ 12 %). The procedural blank varied between 9 and 32 pg Nd ($n = 3$), corresponding to $<$0.02 ‰ of the total Nd loaded.

Table 1
Chemical procedure for neodymium separation.

Elution step	Acid	Volume
Step 1: Cation exchange separation procedure 2 ml AG50W-X8 resin (200–400 mesh) in 10 ml-Bio-Rad columns		
Condition column	2.5 M HCl	10 ml
Load sample	2.5 M HCl	1.5 ml
Discard matrix	2.5 M HCl	12 ml
Discard Ba	2 M HNO_3	8 ml
Collect REE	6 M HCl	13 ml
Clean column	6 M HCl	20 ml
Rince and store	Mill-Q H_2O	20 ml
Step 2: Redox-based separation procedure 0.5 ml LN resin (50–100 μm) in 2 ml-Bio-Rad columns		
Condition column	10 M HNO_3	6 ml
Load sample + collect REE	10 M HNO_3 + 20 mM $NaBrO_3$	0.5 ml
Collect REE	10 M HNO_3 + 20 mM $NaBrO_3$	4 ml
Discard Ce	6 M HCl + 20 mM H_2O_2	5 ml
Discard Ce	6 M HCl	2 ml
Clean column	6 M HCl	10 ml
Clean column	10 M HNO_3	8 ml
Rince and store	0.05 M HCl	8 ml
Step 3: Cation exchange separation procedure 1 ml AG50W-X8 resin (200–400 mesh) in 10 ml-Bio-Rad columns		
Condition column	2.5 M HCl	5 ml
Load sample	2.5 M HCl	0.3 ml
Discard matrix	2.5 M HCl	6.2 ml
Discard Ba	2 M HNO_3	6.5 ml
Collect REE	6 M HCl	7 ml
Clean column	6 M HCl	10 ml
Rince and store	Mill-Q H_2O	10 ml
Step 4: Specific separation procedure 0.82 ml LN resin (20–50 μm) in custom quartz columns (0.4 cm inner diameter)		
Condition column	0.2 M HCl	10 ml
Load sample	0.2 M HCl	0.5 ml
Discard Light REE	0.2 M HCl	6 ml
Collect Nd	0.25 M HCl	5 ml
Discard Heavy REE and clean column	6 M HCl	15 ml
Rince and store	0.05 M HCl	7 ml

2.3. Neodymium isotope measurements by TIMS

Neodymium isotopes were measured on the Nu TIMS at IPGP, following the protocol established in Luu et al. (2022) but optimised for high-precision $^{142}Nd/^{144}Nd$ measurements.

We used zone-refined rhenium filaments (purity of 99.999 % – 0.0012″ × 0.030″) arranged in a double filament setup. The filaments were previously outgassed for 60 min at 4.5 A, using incremental 0.1 A heating steps and a final flash current of 5 A. The loading procedure consisted in a prior deposit of 0.5 μl of 1 M H_3PO_4 heated at 0.8 A followed by about 800 ng of Nd dissolved into 2.5 M HCl. The sample-H_3PO_4 mixture was subsequently slowly evaporated at 0.8 A before being flashed at ≈2.2 A. The optimal run conditions involved an initial intense heating of the ionisation filament (4000–4800 mA, at 600 mA/min) to 1850–1950 °C, followed by progressive heating (500–1100 mA, at 120–240 mA/min) of the evaporation filament until a stable $^{142}Nd^+$ signal of ~7 V was obtained. This signal intensity was maintained at a ± 10 % level by inter-block heating of the evaporation filament in order to have a stable evolution of mass fractionation during the analysis.

Figure 1a shows how 14 out of the 16 Faraday cups of the Nu TIMS were used to dynamically collect all isotopes of Nd, along with $^{140}Ce^+$, $^{141}Pr^+$ and $^{147,149}Sm^+$, over a 5-line cycle, with a one-mass unit step between each line. Each cup was connected to a 10^{11} Ω amplifier. As the position of the Faraday cups is fixed, for each individual line, specific currents were applied to the zoom optics lenses (i.e., Quad 1 and Quad 2 in Fig. 1a) in order to adjust the ion beams toward the Faraday cups. Each line of measurement was integrated for 10 s after a 3-s idle time to stabilise the magnet. The five lines define a cycle and a typical analysis consists in 40 blocks of 20 cycles, with a 3-min baseline measurement between blocks to precisely estimate the instrumental noise. Lens stack parameters were re-tuned every three blocks and the signal peak was re-centred every six blocks. An additional cycle was measured at the beginning of each block to optimize time drift corrections (see discussion in section 3.3.1). The combination of all these analytical conditions led to a cumulative measurement duration of about 18 h.

All Nd isotopes being measured on each line, it provides five static values per isotope ratio (denoted static 1 to 5), whose arithmetic mean gives a multi-static ratio. The multi-line technique also allows the measurement of Nd isotope ratios in common Faraday cups to obtain a dynamic ratio. For example, the dynamic 1 $^{142}Nd/^{144}Nd$ ratio is obtained by combining signals for $^{142}Nd^+$ and $^{144}Nd^+$ measured in the Axial cup on lines 1 and 3 and similarly for $^{144}Nd^+$ and $^{146}Nd^+$ in the H2 cup (Fig. 1b). Similarly, the dynamic 2 and 3 $^{142}Nd/^{144}Nd$ ratios are obtained from the combinations of lines 2 + 4 and 3 + 5, respectively (see Fig. 1b). The arithmetic mean of these three dynamic ratios gives a multi-dynamic ratio. Such combination mathematically cancels approximately 99.6 % of the cup efficiency differences as demonstrated by Di et al. (2021) for multi-dynamic Sr isotope analyses by TIMS. The equations for calculating the dynamic ratios are described in Luu et al. (2022) and build on those described in Garçon et al. (2018) (see Supplementary material for equations). We average the three calculated dynamic ratios for each cycle and then average all multi-dynamic ratios (same as the "mean multi-dynamic" of Di et al., 2021), while other authors average all dynamic ratios together (i.e., "mean all dynamic" in Garçon et al., 2018). Both calculations yield similar results within error (details in the Supplementary Material).

The data are subjected to a series of corrections made either online using the Nu TIMS software, or offline using a Microsoft Office Excel template spreadsheet, provided in the Supplementary Table 2: (1) baseline subtraction from the raw signals; (2) Sm^+ interference correction; (3) time drift correction; (4) mass fractionation correction assuming an exponential law (Thirlwall, 1991) and using $^{146}Nd/^{144}Nd = 0.7219$.

2.4. Definitions and notations

Neodymium isotope variations are small and thus require specific notations in order to ease their observation. In the following, we express the $^{142}Nd/^{144}Nd$, $^{145}Nd/^{144}Nd$, $^{148}Nd/^{144}Nd$ and $^{150}Nd/^{144}Nd$ ratios in the mu notation, as the deviation from a reference composition for the terrestrial mantle, here the average JNdi-1 composition, in parts per million (ppm). They are calculated using the expression $\mu^{x}Nd = (^{X}Nd/^{144}Nd_{sample}/^{X}Nd/^{144}Nd_{JNdi\text{-}1})\ \text{-}1) \times 10^6$. The $^{143}Nd/^{144}Nd$ ratios are expressed in the epsilon notation relative to the CHUR value reported by Bouvier et al. (2008 – $^{143}Nd/^{144}Nd_{CHUR} = 0.512630$ – within error of the original value of Jacobsen and Wasserburg, 1980; Wasserburg et al., 1981) following the equation $\varepsilon^{143}Nd = (^{143}Nd/^{144}Nd_{sample}/^{143}Nd/^{144}Nd_{CHUR})\ \text{-}1) \times 10^4$.

We use the term "reproducibility" when evaluating the long-term dispersion of measurements and it is quantified as 2-standard

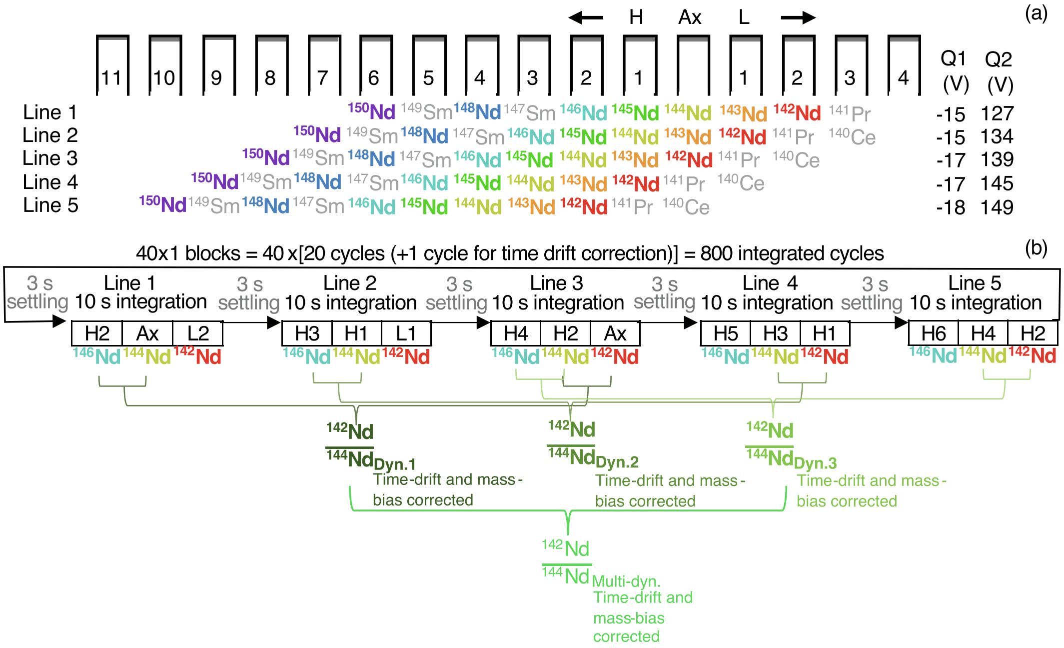

Fig. 1. (a) Cup configuration and (b) analytical procedure used for the 5-line multi-dynamic acquisition method on the Nu TIMS.

deviation on n independent analyses. In contrast, for a single isotopic analysis, we use the term “precision” that corresponds to the 2-standard error on the n cycles of an individual analysis. Reproducibility is therefore a measure of how well data can be trusted on the long term while precision represents a measure of how good a single run is.

3. Improved errors for synthetic standard analyses

Below, we discuss the choices made in terms of running conditions and data reduction protocols to obtain the best possible internal and external errors.

3.1. Results on the two synthetic standards

We performed repeated analyses of the JNdi-1 and AMES Rennes Nd pure standard solutions over a 35-month period (see Fig. 2). Data are separated in two analytical sessions marked by the change of Faraday cups in July 2022. Session 1 lasted for 16 months (March 2021–June 2022) and session 2 for 19 months (July 2022–February 2024), totalling 34 measurements of AMES Rennes Nd (17 during each session) and 25 measurements of JNdi-1 (session 2 only). The average isotope ratios obtained using all techniques (static, multi-static (MS), dynamic and multi-dynamic (MD)) are given in Table 2 and Supplementary Table 1a, b provide additional details.

Each individual measurement performed during this study shows low analytical error, with typical 2se of 1.4, 1.3, 1.1, 2.1 and 3.4 ppm for multi-dynamic ^{142}Nd/^{144}Nd, ^{143}Nd/^{144}Nd, ^{145}Nd/^{144}Nd, ^{148}Nd/^{144}Nd and ^{150}Nd/^{144}Nd ratios (see Supplementary Table 1a). For JNdi-1, we obtain a mean multi-dynamic (MD) value of 1.1418299 ± 36 (2sd, 3.2 ppm, $n = 25$) for ^{142}Nd/^{144}Nd$_{MD}$ and of 0.5121007 ± 10 (2sd, 2.0 ppm) for ^{143}Nd/^{144}Nd$_{MD}$ (Fig. 2), values that are within error of previous high-precision estimates (Fig. 3). For AMES Rennes Nd, measurements during session 1 and 2 give slightly different ^{142}Nd/^{144}Nd$_{MD}$ at 1.1418341 ± 32 (2sd, 2.8 ppm, $n = 17$) and 1.1418291 ± 44 (2sd, 3.9 ppm, n = 17) and ^{143}Nd/^{144}Nd$_{MD}$ at 0.5119498 ± 29 (2sd, 5.7 ppm) and 0.5119586 ± 20 (2sd, 3.9 ppm – see Fig. 2), values that remain similar within error to those published in Luu et al. (2022) (0.511954 ± 2 – 4.3 ppm – see Fig. 3). In summary, Fig. 3 illustrates that the reproducibility obtained here for ^{142}Nd/^{144}Nd ratios compares favourably to other high-precision Nd isotope data measured using TIMS or MC-ICP-MS. The values obtained for the other Nd isotope ratios are also comparable to published values but the reproducibility is about 1.5 to 2.5 times better than most studies, with typical values better than 3.1 ppm for ^{145}Nd/^{144}Nd$_{MD}$, 6.3 ppm for ^{148}Nd/^{144}Nd$_{MD}$ and 13.0 ppm for ^{150}Nd/^{144}Nd$_{MD}$ (see Table 2 and Figs. 2 and 3).

3.2. Optimised run conditions

3.2.1. Cancelling cup bias: The advantage of the 5-line multi-dynamic method

During this study, all static, multi-static, dynamic and multi-dynamic ratios were measured for JNdi-1 and AMES Rennes Nd standards using the 5-line acquisition method. In Fig. 4, we focus on the evolution of measured ^{142}Nd/^{144}Nd ratios over time. During the first session (March 2021 to June 2022), static and multi-static ^{142}Nd/^{144}Nd ratios shown in Fig. 4a reveal a noticeable drift (+25 to −60 ppm), with the difference between the individual static ratios increasing over time as the cups aged. We decided to replace the Faraday cups even though the multi-static average changed by only −3 ppm. During the second period (July 2022 to March 2024), the individual static ratios drifted less (<30 ppm) but the multi-static ratio decreased by a larger amount (≈10 ppm) because the majority of static ratios decreased during this period, while

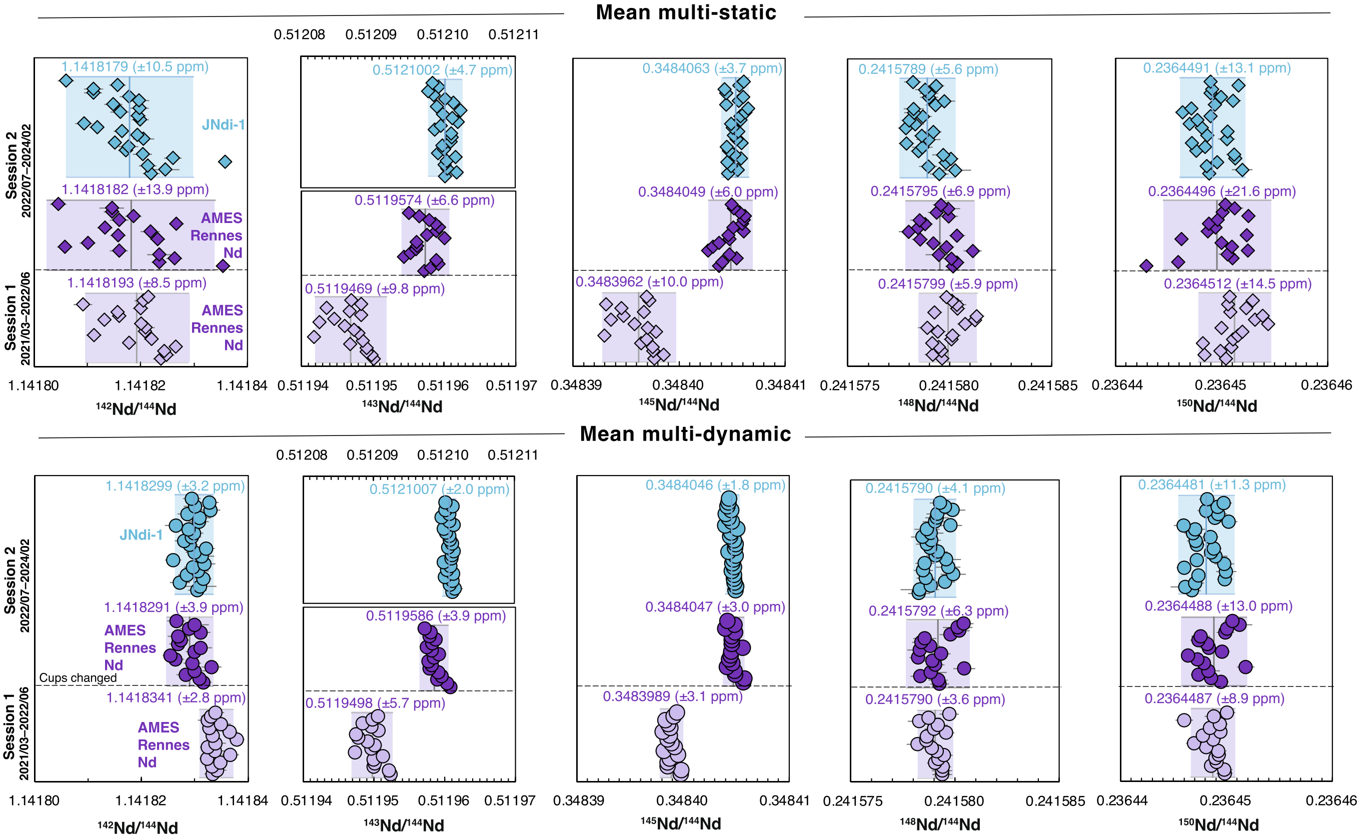

Fig. 2. ^{142}Nd/^{144}Nd, ^{143}Nd/^{144}Nd, ^{145}Nd/^{144}Nd, ^{148}Nd/^{144}Nd and ^{150}Nd/^{144}Nd multi-static and multi-dynamic ratios measured for JNdi-1 and AMES Rennes Nd standards during sessions 1 and 2 in this study, with their associated error bars (2se). Vertical lines represent the mean value of the session and the shaded areas represent the reproducibility of measurements over the session (2sd).

Table 2

Neodymium isotope compositions for JNdi-1 and AMES Rennes Nd standards, reported as the mean value and reproducibility (2sd) on multiple measurements during sessions 1 and 2 of this study.

	^{142}Nd/^{144}Nd	±2sd (×10^{-7})	±2sd ppm	^{143}Nd/^{144}Nd	±2sd (×10^{-7})	±2sd ppm	^{145}Nd/^{144}Nd	±2sd (×10^{-7})	±2sd ppm	^{148}Nd/^{144}Nd	±2sd (×10^{-7})	±2sd ppm	^{150}Nd/^{144}Nd	±2sd (×10^{-7})	±2sd ppm
JNdi-1 (session 2 – n = 25)															
Static 1	1.1418138	245	21.5	0.5120971	84	16.4	0.3484058	47	13.4	0.2415749	78	32.4	0.2364423	102	43.2
Static 2	1.1418215	223	19.6	0.5121043	79	15.5	0.3484037	53	15.2	0.2415715	56	23.4	0.2364398	85	36.0
Static 3	1.1418089	384	33.6	0.5120957	132	25.8	0.3484101	52	14.9	0.2415833	97	40.0	0.2364588	157	66.5
Static 4	1.1417953	276	24.2	0.5120906	109	21.2	0.3484001	72	20.6	0.2415843	49	20.1	0.2364593	74	31.3
Static 5	1.1418504	453	39.7	0.5121134	140	27.2	0.3484071	108	31.0	0.2415805	54	22.5	0.2364457	128	54.3
Multi-static	1.1418179	120	10.5	0.5121002	24	4.7	0.3484053	13	3.7	0.2415789	14	5.6	0.2364491	31	13.1
Dynamic 1	1.1418293	41	3.6	0.5121012	14	2.7	0.3484050	9	2.6	0.2415792	13	5.3	0.2364467	31	13.2
Dynamic 2	1.1418306	62	5.5	0.5121004	13	2.6	0.3484046	8	2.3	0.2415789	13	5.2	0.2364487	26	11.0
Dynamic 3	1.1418299	44	3.8	0.5121004	13	2.6	0.3484042	8	2.2	0.2415791	14	5.6	0.2364491	34	14.4
Multi-dynamic (11-cycle TDC)	**1.1418299**	**36**	**3.2**	**0.5121007**	**10**	**2.0**	**0.3484046**	**6**	**1.8**	**0.2415790**	**10**	**4.1**	**0.2364481**	**27**	**11.3**
Multi-dynamic (2-cycle TDC)	1.1418300	37	3.3	0.5121007	11	2.2	0.3484046	6	1.8	0.2415790	10	4.2	0.2364482	27	11.3
Multi-dynamic (no TDC)	1.1418266	45	4.0	0.5121002	12	2.3	0.3484047	7	1.9	0.2415784	12	4.9	0.2364461	33	14.0
AMES Rennes Nd (session 2 – n = 17)															
Static 1	1.1418113	385	33.7	0.5119518	141	27.6	0.3484068	63	18.2	0.2415789	107	44.2	0.2364478	124	52.2
Static 2	1.1418133	251	22.0	0.5119611	122	23.8	0.3484028	83	23.9	0.2415734	88	36.3	0.2364433	130	55.1
Static 3	1.1418249	529	46.3	0.5119585	172	33.5	0.3484087	91	26.2	0.2415811	133	55.0	0.2364548	204	86.1
Static 4	1.1418025	417	36.5	0.5119490	203	39.7	0.3484029	108	30.9	0.2415840	52	21.4	0.2364599	121	51.3
Static 5	1.1418397	601	52.6	0.5119668	204	39.8	0.3484033	155	44.4	0.2415802	77	32.1	0.2364397	481	203
Multi-static	1.1418182	158	13.9	0.5119574	34	6.6	0.3484049	21	6.0	0.2415795	17	6.9	0.2364496	51	21.6
Dynamic 1	1.1418277	53	4.6	0.5119590	21	4.1	0.3484052	12	3.4	0.2415794	20	8.4	0.2364473	42	17.6
Dynamic 2	1.1418297	55	4.9	0.5119584	26	5.0	0.3484047	11	3.1	0.2415791	17	7.0	0.2364496	36	15.1
Dynamic 3	1.1418299	53	4.7	0.5119584	18	3.6	0.3484043	11	3.1	0.2415792	22	9.0	0.2364496	38	16.2
Multi-dynamic (11-cycle TDC)	**1.1418291**	**44**	**3.9**	**0.5119586**	**20**	**3.9**	**0.3484047**	**10**	**3.0**	**0.2415792**	**15**	**6.3**	**0.2364488**	**31**	**13.0**
Multi-dynamic (2-cycle TDC)	1.1418291	45	3.9	0.5119586	20	4.0	0.3484047	10	2.9	0.2415791	15	6.3	0.2364489	34	14.3
Multi-dynamic (no TDC)	1.1418257	63	5.6	0.5119580	22	4.2	0.3484049	10	3.0	0.2415795	17	6.9	0.2364496	51	21.6
AMES Rennes Nd (session 1 – n = 17)															
Static 1	1.1417446	878	76.9	0.5119160	338	66.1	0.3483847	165	47.3	0.2415887	112	46.5	0.2364639	173	73.1
Static 2	1.1418284	227	19.9	0.5119769	230	45.0	0.3483993	60	17.2	0.2415755	36	14.9	0.2364433	67	28.4
Static 3	1.1418778	539	47.2	0.5119437	159	31.1	0.3483990	58	16.7	0.2415773	119	49.2	0.2364461	169	71.5
Static 4	1.1418222	165	14.5	0.5119480	105	20.5	0.3484028	80	22.9	0.2415795	37	15.4	0.2364538	62	26.1
Static 5	1.1418226	597	52.3	0.5119505	196	38.3	0.3483954	116	33.3	0.2415787	78	32.2	0.2364493	124	52.5
Multi-static	1.1418193	98	8.5	0.5119469	50	9.8	0.3483962	35	10.0	0.2415799	14	5.9	0.2364512	34	14.5
Dynamic 1	1.1418312	40	3.5	0.5119495	46	9.0	0.3483973	22	6.2	0.2415789	13	5.5	0.2364466	22	9.4
Dynamic 2	1.1418387	56	4.9	0.5119480	39	7.7	0.3483994	9	2.6	0.2415789	13	5.3	0.2364493	24	10
Dynamic 3	1.1418320	43	3.8	0.5119518	17	3.2	0.3483999	7	1.9	0.2415793	11	4.8	0.2364504	23	9.9
Multi-dynamic (11-cycle TDC)	**1.1418341**	**32**	**2.8**	**0.5119498**	**29**	**5.7**	**0.3483989**	**11**	**3.1**	**0.2415790**	**9**	**3.6**	**0.2364487**	**21**	**8.9**
Multi-dynamic (2-cycle TDC)	1.1418340	35	3.1	0.5119497	28	5.6	0.3483988	11	3.1	0.2415791	8	3.5	0.2364487	19	8.0
Multi-dynamic (no TDC)	1.1418313	43	3.8	0.5119493	31	6.0	0.3483990	11	3.1	0.2415784	11	4.7	0.2364470	29	12

All static, multi-static, dynamic and multi-dynamic ratios were obtained with the 5-line acquisition method. We favour the mean of time-drift corrected (TDC) multi-dynamic ratios using the 11-cycle interpolation (11-cycle TDC) reported in bold. Mean multi-dynamic ratios time-drift corrected using a 2-cycle interpolation (2-cycle TDC) and uncorrected for time drift (no TDC) are reported for comparison.

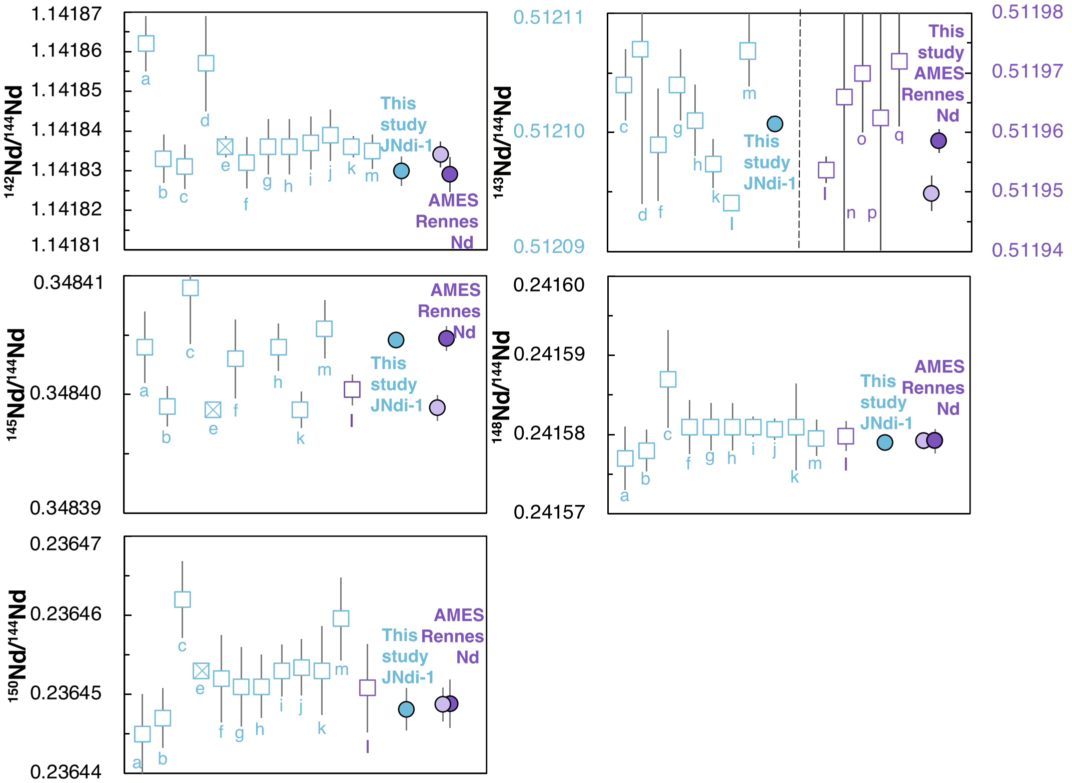

Fig. 3. ^{142}Nd/^{144}Nd, ^{143}Nd/^{144}Nd, ^{145}Nd/^{144}Nd, ^{148}Nd/^{144}Nd and ^{150}Nd/^{144}Nd ratios measured on synthetic reference materials in this study (filled symbols), and comparison with literature data (open symbols), and their respective reproducibility (error bars – 2sd). Literature data are from (a) Boyet and Carlson, 2005, (b) Andreasen and Sharma, 2009, (c) Gannoun et al., 2011, (d) Ali and Srinivasan, 2011, (e) Saji et al., 2016 (MC-ICP-MS), (f) Garçon et al., 2018, (g-h) Pin and Gannoun, 2019a, 2019b, (i-j) Fukai et al., 2017, Fukai and Yokoyama, 2019, (k) Hyung and Tissot, 2021, (l) Luu et al., 2022, (m) Peters et al., 2024 for JNdi-1, and (l) Luu et al., 2022, (n) Le Fèvre and Pin, 2005, (o) Weis et al., 2006, (p) Chauvel et al., 2011, (q) Fourny et al., 2016 for AMES Rennes Nd.

it was not the case during session 1. In contrast, the three dynamic and multi-dynamic ratios hardly changed within both sessions (Fig. 4b), highlighting the effectiveness of the dynamic method as previously shown by Caro et al. (2006) and Roth et al. (2013, 2014).

At any given time in Fig. 4b, the three dynamic ^{142}Nd/^{144}Nd ratios differ by 6.5 ppm or less but they are not identical. This indicates, as pointed out by Roth et al. (2014), that the difference in cup efficiency is not completely cancelled out by the procedure. This is particularly evident in session 1 during which the difference between the three dynamic averages increases over the 1.5-year time period (Fig. 4b). To mitigate this residual bias, several studies have combined two dynamic ratios into a multi-dynamic ratio (e.g., Garçon et al., 2018; Di et al., 2021). Here, we take advantage of the 5-line acquisition method to generate a multi-dynamic ^{142}Nd/^{144}Nd ratio based on the three dynamic ratios and which is even less affected by bias due to differences in cup efficiency. The calculated multi-dynamic ^{142}Nd/^{144}Nd ratios represented in Fig. 4b remain virtually constant over the entire length of each session providing stable and precisely-determined values. The multi-dynamic ratios similarly calculated for all the other Nd isotopes also show stable and precise values over time (see Table 2 and Supplementary Table 1a).

3.2.2. *Improving counting statistics and signal-to-noise ratio*

The relationship between analytical error and run duration was investigated by Garçon et al. (2018 – see their Fig. 3) and Luu et al. (2019, 2022) based on Johnson-Nyquist noise and counting statistics. Improving precision requires therefore improving counting statistics and signal-to-noise ratio. In other words, higher Nd^{+} intensity and longer analyses translate into lower standard errors. In Fig. 5, we plot the 2se obtained on multi-dynamic ^{142}Nd/^{144}Nd ratios for 59 independent runs against signal intensity on ^{142}Nd^{+}, and use a colour scale to illustrate the number of cycles. Our dataset clearly shows that increasing the ^{142}Nd^{+} signal from 4 to 9 V or extending the analysis from 400 to 800 cycles reduces the standard error by 0.6 ppm, as predicted by theory.

In this study, we make a compromise between very long and very high intensity analyses and choose to measure at ~7 V of ^{142}Nd^{+} for 800 cycles, achieving an average 2se of ~1.4 ppm. This requires ~800 ng of Nd loaded on the filament and an 18-h run. To our knowledge, these are the longest TIMS analyses at such high intensities (e.g., ~8 h at 4–8 V of ^{142}Nd^{+} in Garçon et al., 2018; Hyung and Tissot, 2021; Luu et al., 2022) while using less than 1000 ng of Nd. Such performance results most probably from the combination of various factors (use of high-purity zone refined 99.999 % Re filaments, consistent loading and heating procedures, efficient tuning process and excellent vacuum in the source – ~1×10^{-8} mbar during the measurement, without the use of liquid nitrogen – and the fly tube – ~2×10^{-9} mbar).

3.3. *Improving data reduction*

3.3.1. *Time drift correction*

In multi-dynamic measurements, dynamic Nd isotope ratios are measured at different times t, during different acquisition lines. However, Nd isotope ratios evolve over time during TIMS analyses (Roth et al., 2014). Therefore, they require to be corrected for time drift in order to estimate their value at the same time t. To do this, the fractionation rate of each ratio is estimated from several neighbouring cycles and is then used to interpolate the value of the isotope ratio at a time t corresponding to the first line of the block. Based on studies by Garçon et al. (2018), Di et al. (2021) and Luu et al. (2022), we tested two interpolation methods: over 2 cycles (n-1 to n) and over 11 cycles (n-5 to n + 5). The Nu TIMS software includes an online 2-cycle interpolation,

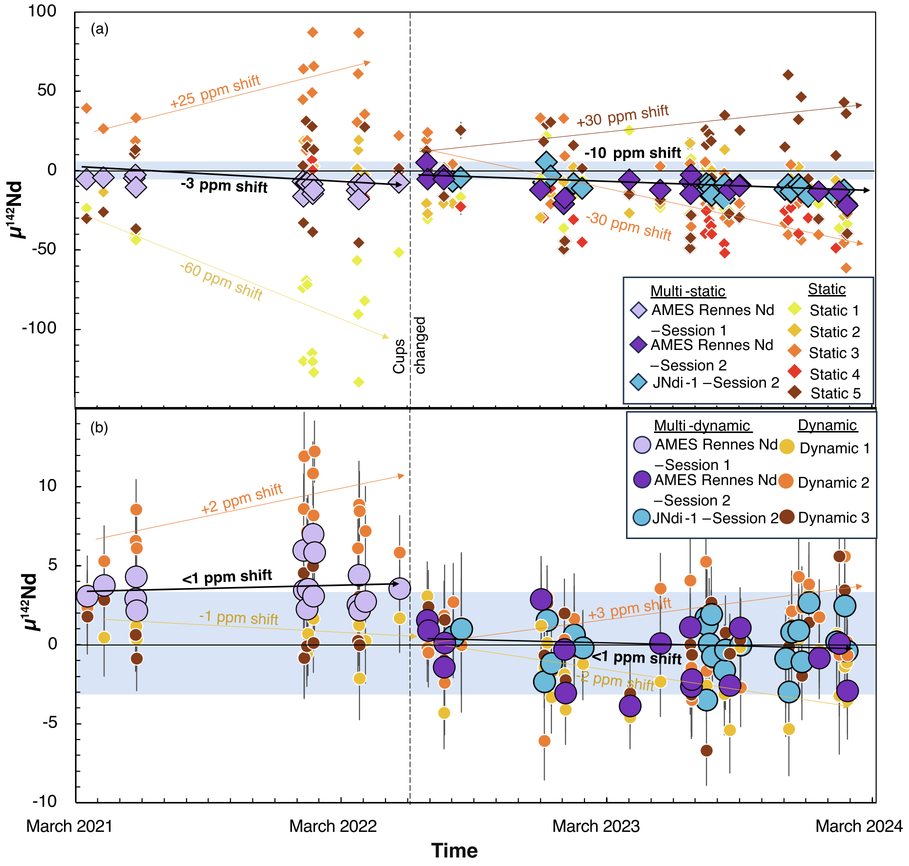

Fig. 4. Time vs. (a) static and multi-static $^{142}Nd/^{144}Nd$ ratios and (b) dynamic and multi-dynamic $^{142}Nd/^{144}Nd$ ratios measured in JNdi-1 and AMES Rennes Nd synthetic reference materials during the two analytical sessions, separated by a cup change in July 2022. All ratios are reported in the mu notation relative to the average multi-dynamic $^{142}Nd/^{144}Nd$ ratio measured for JNdi-1. Error bars are the internal error (2se) on the individual measurements. Blue shaded areas represent the reported 2sd on the multi-dynamic $^{142}Nd/^{144}Nd$ ratio for JNdi-1 in this study (~3 ppm), as a reference. Coloured arrows illustrate the typical shift observed overtime on the static 1 (yellow diamond), static 3 (orange diamond), static 5 (brown diamond), multi-static (bold), dynamic 1 (yellow dot), dynamic 2 (orange dot) and multi-dynamic ratios (bold). (For interpretation of the references to colour in this figure legend, the reader is referred to the web version of this article.)

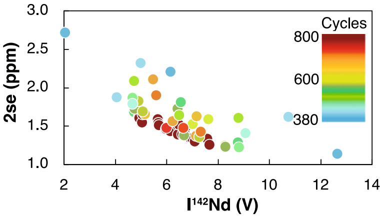

Fig. 5. Mean $^{142}Nd^{+}$ signal ($I^{142}Nd$) vs. 2-standard error (2se) on the mean multi-dynamic $^{142}Nd/^{144}Nd$ ratio from 55 individual JNdi-1 and AMES Rennes Nd analyses acquired during the course of this study. A colour scale indicates the number of integrated cycles for each analysis. Despite the visible overlap of data points, the mean number of cycles per analysis on pure Nd solution is 723.7 cycles for a mean $^{142}Nd^{+}$ signal intensity of 6.51 V.

including an additional cycle at the beginning of each block for interpolation purposes only. The 11-cycle method was applied offline and uses neighbouring cycles, including those from adjacent blocks (see example in Fig. 6a for $^{146}Nd/^{144}Nd$ ratios). The calculations can be found in the Supplementary Table 2.

Figure 6 shows the impact of time drift correction for an 800-cycle analysis. The 11-cycle interpolation method provides a much more stable fractionation rate, reducing the scatter by a factor of 10 compared to the 2-cycle method (see example in Fig. 6b). However, we recognize that some of the information may be lost and local variations in the fractionation rate may be smoothed out. Both methods give similar results at the analysis scale (see Fig. 6c for $^{142}Nd/^{144}Nd$) and at the dataset scale (Table 2 and Supplementary Table 1a,e) with <1 ppm differences in Nd isotope ratios and comparable reproducibility for AMES Rennes Nd and JNdi-1 measurements. The 11-cycle interpolation was adopted for final reporting in this study although both methods are equivalent.

More importantly, the uncorrected data differ significantly from the time-drift corrected data, as illustrated by lower $^{142}Nd/^{144}Nd$ ratios in Fig. 6c. At the dataset scale, corrected data are more reproducible (e.g., Table 2 and Supplementary Table 1a,f) and more consistent with published reference compositions (Fig. 3). Finally, the difference between uncorrected and corrected values increases with increasing fractionation rate. For $^{148}Nd/^{144}Nd$ and $^{150}Nd/^{144}Nd$ ratios, the difference reaches up to 8.2 and 26 ppm on individual measurements (see Supplementary Table 1a,f), whereas for $^{142}Nd/^{144}Nd$ and $^{145}Nd/^{144}Nd$ ratios, it only reaches up to 3.1 and 0.9 ppm. These observations emphasize the importance of time-drift correction for high-precision analyses.

3.3.2. Removal of outliers

The removal of outliers using a 2σ filter during data processing is common and usually integrated in mass spectrometer software. In this study, the automated 2σ filter applied to the multi-dynamic ratios (see calculations in Supplementary Table 2) significantly improves precision. For a typical run of 800 cycles, the 2σ filter removes about 4 % of the ratios and improves the analytical error and the reproducibility by about 14 %.

In addition, we use four objective criteria to ensure the reliability of

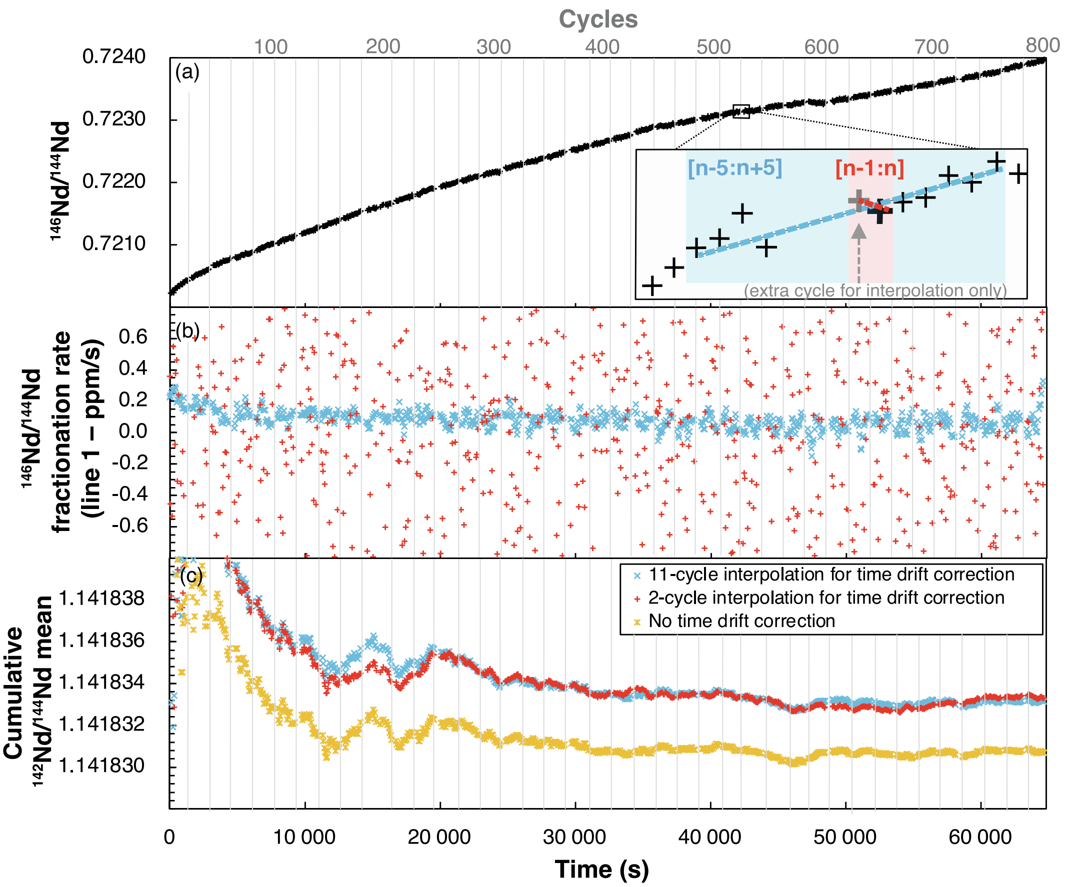

Fig. 6. Neodymium isotope composition evolution over the analysis of AMES Rennes #23. Panels (a) and (b) show the evolution of the ^{146}Nd/^{144}Nd isotope ratio relative to the value measured on acquisition line 1 and its fractionation rate, estimated by interpolation over 11 cycles (blue symbols) or 2 cycles (red symbols). Panel (c) represents the evolution of the cumulative mean multi-dynamic ^{142}Nd/^{144}Nd ratio, without (yellow) and with time-drift correction using 11-cycles or 2-cycles interpolations of the fractionation rate (blue and red). (For interpretation of the references to colour in this figure legend, the reader is referred to the web version of this article.)

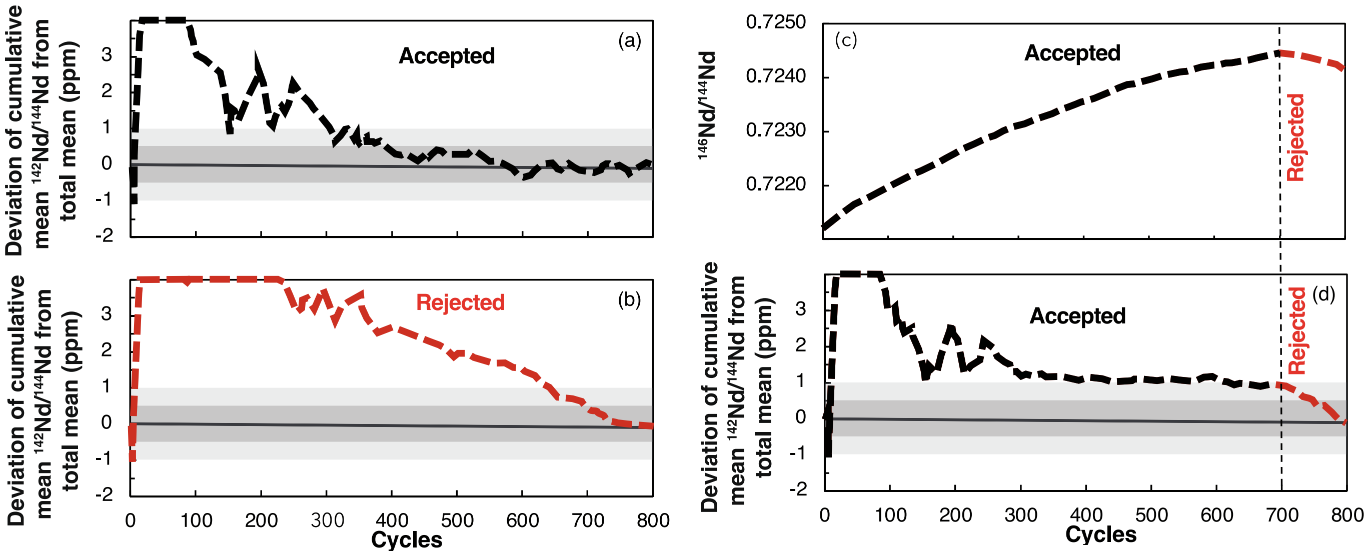

Fig. 7. Evolution of measured values for ^{142}Nd/^{144}Nd and ^{146}Nd/^{144}Nd over 800 cycles. Panel (a) shows how the deviation from the final average of the cumulative mean multi-dynamic ^{142}Nd/^{144}Nd evolves for a typical good run with a stable plateau for 400 cycles; panel (b) shows a run that is rejected due to the absence of stable plateau; panel (c) illustrates a case when the ^{146}Nd/^{144}Nd isotope ratio shows a reverse evolution at the end of the run, creating a destabilisation of the plateau in panel (d). In panel (d), only the last 100 cycles are rejected. Deviation limits are represented as ± 0.5 ppm (dark grey shaded band) and ± 1 ppm (light grey shaded band).

the results:

1) First, we eliminate any run whose internal error exceeds 3 ppm on the $^{142}Nd/^{144}Nd$ ratio. In practice, this eliminates analyses with less than 400 cycles.
2) Secondly, as suggested by Garçon et al. (2018), we reject analyses in which the cumulative mean $^{142}Nd/^{144}Nd$ does not converge to a plateau. Here, the plateau is judged acceptable if the cumulative mean multi-dynamic $^{142}Nd/^{144}Nd$ ratio remains within 0.5 ppm of its final value for at least 200 cycles or 1 ppm for at least 400 cycles. A typical good run is shown in Fig. 7a while an example of a rejected run is shown in Fig. 7b. During the course of this study, a dozen out of 95 analyses never reached a plateau and were rejected.
3) We also reject analyses with a chaotic mass fractionation evolution or truncate analyses with reverse mass fractionation. Normally, the $^{146}Nd/^{144}Nd$ ratio evolves steadily from ~0.7200 to ~0.7240 (Fig. 6a) but sometimes, it is not the case. For instance, analyses whose $^{146}Nd/^{144}Nd$ ratio eventually exceeds 0.7240 frequently show a subsequent reverse isotope fractionation as illustrated in Fig. 7c. It usually generates abnormal variations of the Nd isotope ratios, as illustrated in Fig. 7d. In this study, seven out of 95 analyses showed such effect and they were truncated by 40 to 100 cycles.
4) Finally, we examine the difference between static ratios and eliminate an entire run if the five static ratios differ too much from each other. For example, when the typical difference between the five $^{142}Nd/^{144}Nd$ static ratios was about 75 ppm in March 2022 (see Fig. 4a), two analyses had differences of ~400 ppm at that time and were rejected.

Following these four criteria, fourteen analyses out of 95 were

Table 3
Neodymium isotope compositions of USGS and GIT-IWG rock reference materials measured during the course of this study.

Sample	Session	$\mu^{142}Nd$	±2se/ **2sd**	$^{143}Nd/^{144}Nd$	±2se/ sd ($\times10^{-7}$)	$\varepsilon^{143}Nd$	±2se/ **2sd**	$\mu^{145}Nd$	±2se/ **2sd**	$\mu^{148}Nd$	±2se/ sd	$\mu^{150}Nd$	±2se/ **2sd**	Recov. yield
BHVO-2 #1	1	−4.8	1.7	0.5129718	7	6.67	0.01	0.7	1.1	−2.8	2.2	−8.9	3.4	/
BHVO-2 #2 (dup.1)	1	−1.9	1.5	0.5129713	7	6.66	0.01	−0.7	1.2	3.9	2.0	−1.1	3.3	96 %
BHVO-2 #3 (dup.1,rep.)	2	3.7	1.4	0.5129735	6	6.70	0.01	2.1	1.0	−0.8	1.8	−2.1	2.9	96 %
BHVO-2 #4 (dup.2)	2	7.8	1.6	0.5129729	7	6.69	0.01	−1.9	1.1	5.2	2.2	17.1	3.4	93 %
BHVO-2 #5 (dup.2,rep.)	2	2.7	2.1	0.5129728	9	6.69	0.02	−1.8	1.4	7.0	2.7	14.0	4.6	93 %
BHVO-2 #6 (dup.2,rep.)	2	1.4	1.8	0.5129730	8	6.69	0.01	−0.1	1.3	2.9	2.4	4.7	3.8	93 %
Mean BHVO-2		**1.5**	**8.8**	**0.5129726**	17	**6.68**	**0.03**	**−0.3**	**3.1**	**2.6**	**7.4**	**4.0**	**20.0**	
BCR-2 #1	1	1.9	1.2	0.5126222	5	−0.15	0.01	−1.0	0.9	−0.9	1.6	−15.2	2.7	100 %
BCR-2 #2 (rep.)	2	4.5	1.5	0.5126254	7	−0.09	0.01	4.0	1.1	−3.4	2.1	−9.9	3.3	100 %
BCR-2 #3 (dup.2)	2	0.3	1.5	0.5126212	6	−0.17	0.01	−1.1	1.1	1.3	2.0	0.2	3.1	98 %
BCR-2 #4 (dup.2,rep.)	2	−1.6	2.2	0.5126216	9	−0.16	0.02	0.3	1.5	−0.6	3.1	−1.8	4.7	98 %
BCR-2 #5 (dup.3)	2	5.3	1.7	0.5126165	7	−0.26	0.01	−0.4	1.1	3.2	2.2	17.2	3.5	76 %
Mean BCR-2		**2.1**	**5.9**	**0.5126214**	64	**−0.17**	**0.12**	**0.3**	**4.2**	**−0.1**	**5.0**	**−1.9**	**24.7**	
RGM-1 #1	1	1.0	2.5	0.5127873	10	3.07	0.02	2.6	1.8	−5.2	3.2	−17.3	5.5	100 %
RGM-1 #2 (rep.)	1	2.0	1.7	0.5127847	8	3.02	0.01	0.8	1.3	−3.9	2.1	−15.4	3.7	100 %
RGM-1 #3 (rep.)	2	1.5	1.4	0.5127866	6	3.05	0.01	2.6	1.1	1.4	1.8	−2.7	3.1	100 %
RGM-1 #4 (rep.)	2	5.0	1.4	0.5127875	6	3.07	0.01	2.4	1.1	−3.4	1.8	−8.1	2.9	100 %
Mean RGM-1		**2.4**	**3.6**	**0.5127865**	25	**3.05**	**0.05**	**2.1**	**1.8**	**−2.8**	**5.8**	**−10.9**	**13.5**	
BE-N #1	2	0.2	1.3	0.5128694	6	4.67	0.01	1.8	0.9	0.0	1.8	−1.2	2.7	97 %
BE-N #2 (rep.)	2	1.1	1.3	0.5128696	5	4.67	0.01	0.1	0.9	−1.2	1.9	−2.0	2.8	97 %
BE-N #3 (rep.)	2	2.2	1.3	0.5128700	6	4.68	0.01	0.4	1.0	−0.3	1.8	−1.7	2.9	97 %
BE-N #4 (rep.)	2	2.9	2.1	0.5128704	10	4.69	0.02	1.2	1.6	−1.1	2.7	−7.0	4.6	97 %
BE-N #5 (rep.)	2	2.3	1.7	0.5128698	7	4.68	0.01	−0.3	1.1	0.7	2.3	−2.5	3.6	97 %
Mean BE-N		**1.7**	**2.1**	**0.5128698**	**7**	**4.68**	**0.01**	**0.6**	**1.7**	**−0.4**	**1.6**	**−2.9**	**4.7**	
BIR-1	2	**0.9**	**1.6**	**0.5130787**	**7**	**8.75**	**0.01**	**1.7**	**1.2**	**−5.0**	**2.1**	**−14.9**	**3.3**	**95 %**
AGV-2	2	**2.4**	**2.0**	**0.5127777**	**9**	**2.88**	**0.02**	**−0.5**	**1.4**	**−0.8**	**2.6**	**0.0**	**3.9**	**93 %**

$\mu^{x}Nd = ((^{x}Nd/^{144}Nd_{sample}/^{x}Nd/^{144}Nd_{JNdi\text{-}1}) -1) \times 10^{6}$, JNdi-1 refers to the mean isotope composition of JNdi-1 standard obtained during session 2.
Samples run during session 1 were normalized to session 2 using the correction factor $^{x}Nd/^{144}Nd_{AMES\ session\ 2}/^{x}Nd/^{144}Nd_{AMES\ session\ 1}$ using the mean isotope compositions of AMES Rennes Nd standard measured during the two sessions.
$\varepsilon^{143}Nd = ((^{143}Nd/^{144}Nd_{sample}/^{143}Nd/^{144}Nd_{CHUR}) -1) \times 10^{4}$, with $^{143}Nd/^{144}Nd_{CHUR} = 0.512630$ (Bouvier et al., 2008).
2se: two-standard error (internal error).
2sd: two-standard deviation (reproducibility).
Rep.: replicates, samples that were loaded and analysed multiple times on different filaments
Dup.: duplicates, samples that underwent distinct digestions and chemical procedures.
The reported mean values (bold) represent the average of all replicates and duplicates for each sample.

rejected.

The 5-line multi-dynamic method developed in this study offers three main advantages: (1) For the first time, all Nd isotope ratios are derived from three distinct dynamic measurements whereas previous studies only measured two dynamic ratios for ^{142,143,148}Nd/^{144}Nd and only one dynamic ratio for ^{150}Nd/^{144}Nd (e.g., in Garçon et al., 2018; Peters et al., 2018). This method minimizes bias from cup efficiency differences and improve accuracy and reproducibility down to ≈3 ppm on the ^{142,143,148}Nd/^{144}Nd ratios and ≈13 ppm on the ^{150}Nd/^{144}Nd, which is up to twice as low as recent literature. (2) The method achieves unparalleled analytical precision through 18-h acquisitions of high-intensity Nd signals. (3) An enhanced data reduction procedure maximizes data reliability. Although time-consuming, this method is highly effective in detecting minute variations in Nd isotope ratios that may remain undetected with other analytical techniques.

4. Identification of artefacts for geological samples

4.1. Results on rock reference materials

We applied the analytical method and data reduction scheme described above to five rock reference materials processed through chemistry and report their Nd isotope composition in Table 3. All samples, except BIR-1 and AGV-2, were measured multiple times and BHVO-2 and BCR-2 underwent several distinct digestions and chemical processing. Details about the individual measurements are given in the Supplementary Table 1c,d.

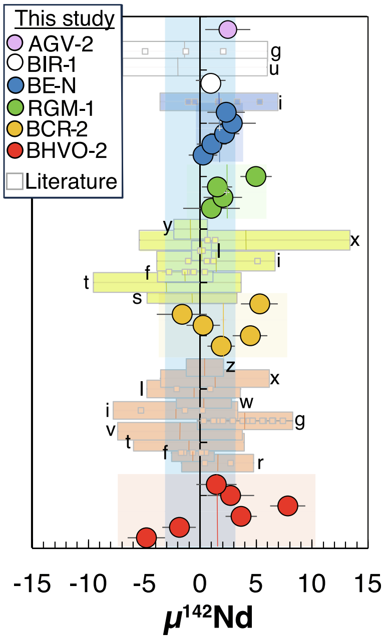

Fig. 8. μ^{142}Nd values of rock reference materials measured in this study (dot symbol), expressed in the mu notation relative to the average ^{142}Nd/^{144}Nd ratio measured for JNdi-1 standard during session 2. Error bars are 2se. Vertical lines represent the mean value on the repeated measurements and shaded areas are 2sd. The light blue shaded area represents the reproducibility on JNdi-1 measurements over session 2 (3 ppm). Recent literature values are reported for comparison, either as a unique measurement or multiple measurements (small squares represent individual measurements) with mean values reported as vertical lines and uncertainty (2sd/2se) as coloured areas with grey surrounding. Literature data are from the studies (a-q) reported in Fig. 4 and (r) Rizo et al., 2011, (s-t) Roth et al., 2013, 2014, (u) Burkhardt et al., 2016, (v) Gautam et al., 2017, (w) Hyung and Jacobsen, 2020, (x) Frossard et al., 2022, (y) Fang et al., 2022, (z) Hasenstab-Dübeler et al., 2022. (For interpretation of the references to colour in this figure legend, the reader is referred to the web version of this article.)

The μ^{142}Nd values of the rock reference materials are shown in Fig. 8. They all have similar and slightly positive μ^{142}Nd values but they remain, within error, undistinguishable from the terrestrial reference (see Table 3 and Fig. 8). Their μ^{142}Nd values are also in excellent agreement with the literature data shown with square symbols in Fig. 8. Similarly, their ^{143}Nd/^{144}Nd ratios listed in Table 3 are similar within error with reference values reported in Zhang and Hu (2020), and with recent high-precision values reported in Pin and Gannoun (2019a, 2019b) and Luu et al. (2022).

The reproducibility on replicate μ^{142}Nd measurements of BE-N (2.8 ppm, $n = 5$) and RGM-1 (3.6 ppm, $n = 4$) is similar to the reproducibility obtained for the pure Nd standards (2.8 to 3.9 ppm for JNdi-1 and AMES Rennes Nd – Table 2 and Fig. 2). However, it is not the case of BCR-2 and BHVO-2 for which the 2sd on μ^{142}Nd reach 5.9 and 8.8 ppm. We interpret the much larger spread as due to the multiple independent digestion and separation procedures (referred as dup. 1 to 3 in Table 3) that they went through. Considering only replicate measurements of the same fraction, the reproducibility is much better (Table 3). Thus, the chemistry procedure seems to affect the reproducibility and we suspect two main causes: either a poor separation of other elements generating isobaric interferences, or an isotope fractionation created by the chemical isolation of Nd. Hereafter, we take advantage of the high-precision measurement of all Nd isotope ratios to evaluate the potential impact of these two factors on the accuracy of the μ^{142}Nd data in natural samples.

4.2. Avoiding isobaric interferences on Nd isotope ratios

To ensure accurate ^{142}Nd isotope measurements, Ce and Sm must be removed by the chemical procedure as ^{142}Ce^{+} and ^{144}Sm^{+} isobarically interfere with ^{142}Nd^{+} and ^{144}Nd^{+}. In addition, their residual presence in the sample loaded on the filament must be monitored by measuring ^{140}Ce^{+} and ^{147}Sm^{+} together with the Nd^{+} signals (see Fig. 1) so that we can evaluate if interference corrections are necessary.

Figure 9a,b illustrates the impact of a small Ce^{+} signal on the ^{142}Nd/^{144}Nd ratio. Here, we model how a ^{140}Ce/^{144}Nd as low as 2.7×10^{-5} (equivalent to ~0.1 mV signal of ^{140}Ce^{+} added to a run with ~5 V of ^{142}Nd^{+}) results in a 3-ppm increase of the ^{142}Nd/^{144}Nd ratio, approaching our reproducibility limit on synthetic standards. This demonstrates that complete removal of Ce in the Nd fraction is essential for accurate results and that monitoring the ^{140}Ce^{+} signal is compulsory. Accordingly, we recommend that ^{140}Ce/^{144}Nd does not exceed 2.7×10^{-5} to keep the Ce contribution on the ^{142}Nd/^{144}Nd ratio negligible compared to reproducibility. In case, readers would like to apply a correction, we would recommend to correct the individual dynamic ratios when ^{140}Ce/^{144}Nd ratio exceeds 9×10^{-6} (≈1-ppm effect on the ^{142}Nd/^{144}Nd ratio).

During the course of this study, the measured ^{140}Ce/^{144}Nd for the rock reference materials was systematically below the threshold (average ^{140}Ce/^{144}Nd $\approx 8 \times 10^{-6}$, see Supplementary Table 1c), with most measurements having interference levels below detection limits. Consequently, we did not apply corrections for Ce^{+} interferences on any of the measured samples. We conclude that, given the observed negligible Ce^{+} signals, the range of μ^{142}Nd obtained for BHVO-2 and BCR-2 is not due to Ce^{+} interferences.

The impact of Sm interferences on the ^{142}Nd/^{144}Nd ratio is also shown in Fig. 9c,d. In that case, a theoretical ^{147}Sm/^{144}Nd of 7.3×10^{-6} (0.03 mV signal of ^{147}Sm^{+} for ~5 V of ^{142}Nd^{+}) results in a 3-ppm decrease of the ^{142}Nd/^{144}Nd ratio. It also impacts all other Nd isotope ratios with decreases of 2.3 and 0.7 ppm for ^{143}Nd/^{144}Nd and ^{145}Nd/^{144}Nd and increases of 18.5 and 17.2 ppm for ^{148}Nd/^{144}Nd and ^{150}Nd/^{144}Nd due to additional ^{148}Sm^{+} and ^{150}Sm^{+}interferences. To avoid a significant effect on ^{142}Nd/^{144}Nd, we recommend ^{147}Sm/^{144}Nd being kept below 7.3×10^{-6} and for an accurate determination of ^{148}Nd/^{144}Nd and ^{150}Nd/^{144}Nd ratios, this threshold should be reduced to 1.4×10^{-6}. In the data reduction spreadsheet provided in the Supplementary Table 2, we set the lower limit for an automated Sm

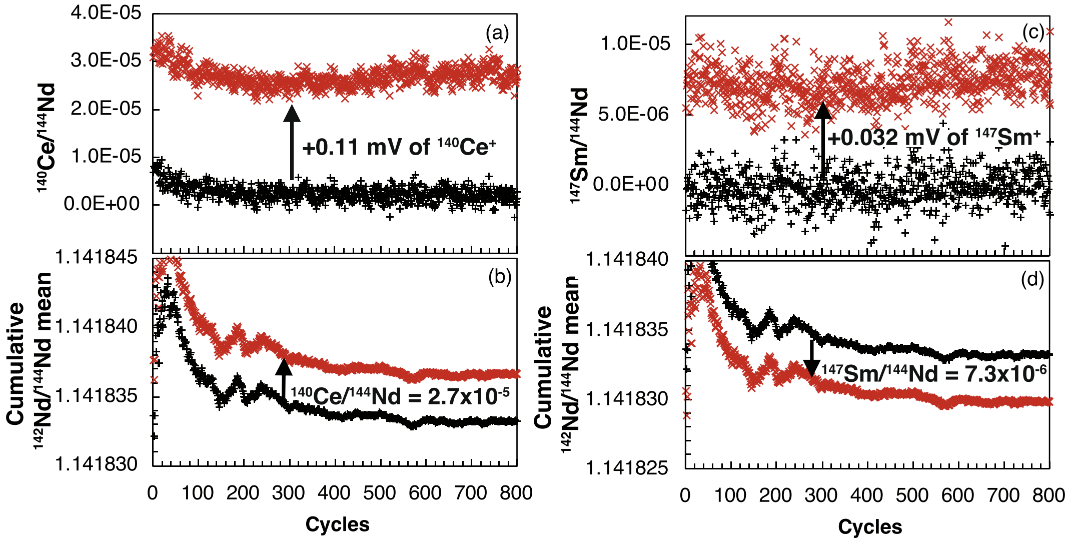

Fig. 9. Cycle-by-cycle comparison of isotope ratios measured during the analysis of AMES Rennes Nd #23 without (black) and with (model – red) the simulation of the impact of isobaric Ce and Sm interferences on ^{142}Nd/^{144}Nd. Panels (a) represents the ^{140}Ce/^{144}Nd ratio for an addition of ~0.1 mV of ^{140}Ce$^+$ for ~5 V of ^{142}Nd$^+$ while panel (b) represents the resulting contribution of Ce$^+$ on the cumulative mean ^{142}Nd/^{144}Nd isotope ratios. Panel (c) represents the ^{147}Sm/^{144}Nd ratio for an addition of ~0.03 mV of ^{147}Sm$^+$ for ~5 V of ^{142}Nd$^+$ while panel (d) represents the resulting contribution of Sm$^+$ on the cumulative mean ^{142}Nd/^{144}Nd isotope ratios. (For interpretation of the references to colour in this figure legend, the reader is referred to the web version of this article.)

interference correction at ^{147}Sm/^{144}Nd = 7.0 × 10^{-7} (≈2-ppm effect on the ^{148}Nd/^{144}Nd and ^{150}Nd/^{144}Nd ratios).

During the course of this study, we detected traces of Sm in JNdi-1 with an average ^{147}Sm/^{144}Nd ratio of 1.8 × 10^{-6}. Such low value has no real impact on ^{142}Nd/^{144}Nd but it requires a Sm interference correction to obtain accurate ^{148}Nd/^{144}Nd and ^{150}Nd/^{144}Nd ratios. In contrast, the intensity of the Sm$^+$ signal is negligible for AMES Rennes Nd (^{147}Sm/^{144}Nd $< 3.8 \times 10^{-8}$) and for most rock reference materials, and none of the Nd isotope ratios is affected. Two samples, BIR-1 and BHVO-2 #3, had ^{147}Sm/^{144}Nd close to the 1.4 × 10^{-6} threshold that could affect ^{148}Nd/^{144}Nd and ^{150}Nd/^{144}Nd ratios and these samples were corrected for Sm interference. Finally, none of the BHVO-2 and BCR-2 measurements had a ^{147}Sm/^{144}Nd larger than 1.8 × 10^{-6} suggesting that Sm interferences are not the cause of the ^{142}Nd/^{144}Nd variability observed in Fig. 8.

4.3. Detecting small nuclear field shift effect on Nd isotopes

While solar system materials carry isotope anomalies of nucleosynthetic origin, terrestrial samples are not expected to exhibit any such effect in their neodymium isotope abundances. Nevertheless, several authors observed it and attributed it to processes occurring during chemical procedures (Fujii et al., 2009; Zheng and Hintelmann, 2010; Cook and Schönbächler, 2016; Yang and Liu, 2016). This was notably confirmed by the strongly fractionated Nd isotope ratios measured in Nd cuts collected at different steps of the chemical procedure on LN resin (Saji et al., 2016). Such effect is called the nuclear field shift (NFS) effect and it was interpreted by Bigeleisen (1996) as due to a mass-independent isotopic fractionation caused by differences in the electric charge distributions among heavy isotopes. This phenomenon has long been ignored due to its small impact compared to analytical uncertainties but, with improved analytical precision, the NFS effect can no longer be neglected for terrestrial samples.

Mass-independent Nd isotope variations due to NFS effect can be estimated using the equation of Fujii et al. (2006, 2009), established Nd mean-squared nuclear charge radii $\langle r^2 \rangle$ values and a NFS intensity expressed as α. Fig. 10a shows Nd isotope spectra for four different sets of Nd mean-squared nuclear charge radii $\langle r^2 \rangle$ values (Angeli, 2004; Fricke and Heilig, 2004; Angeli and Marinova, 2013). For a given α, the four models are quite similar, but not identical, in particular for μ^{142}Nd. When compared to the extremely chemically fractionated Nd cut measured by Saji et al. (2016 – Fig. 10b), it suggests that the best match is a pattern calculated using $\langle r^2 \rangle$ values from Fricke and Heilig (2004) at α = −460. Using these parameters, we can calculate theoretical patterns for various α values (see Figs. 10c,d). Increasingly negative α values result in the increase of μ^{142} and μ^{145} and the decrease of μ^{148} and μ^{150}, while the opposite is observed for positive α values. In practice, a NFS effect of 3 ppm for μ^{142}Nd should entrain a similar shift for μ^{145}Nd, and shifts in the opposite direction of 5 ppm for μ^{148}Nd and 25 ppm for μ^{150}Nd (see Fig. 10c,d).

Because our method provides high-precision determination of all Nd isotope ratios (see Table 2), the data for each rock reference material can be evaluated for potential deviations that could be attributed to NFS effect during chemical separation. As can be seen in Fig. 11, most rock reference materials have Nd isotope patterns showing little to no deviation of their μ^{145}Nd, μ^{148}Nd and μ^{150}Nd from the reference values. However, two RGM-1 (RGM-1 #1 and #2) and one BIR-1 measurements exhibit significantly negative μ^{148}Nd and μ^{150}Nd values, suggesting that their ^{142}Nd/^{144}Nd ratios could potentially be over-estimated by about 2 ppm relative to the true values. In contrast, BHVO-2 #4 and #5 have negative μ^{145}Nd and positive μ^{148}Nd and μ^{150}Nd values, suggesting that their ^{142}Nd/^{144}Nd might potentially be under-estimated by about 2 ppm. Nevertheless, deviations for these five samples remain very small and do not point toward a unique α value, thus preventing quantitative correction of NFS. The shift of μ^{142}Nd value due to NFS is then supposed to be small and within analytical error but data need to be interpreted carefully. Finally, the μ^{150}Nd values of samples BCR-2 #1 and 5 deviate significantly from the error bar but the other ratios remain within error preventing identification of a NFS effect.

Saji et al. (2016) attributed the magnitude of the NFS effect to low Nd recovery during the chemical separation of REE using LN resin. In this study, only BCR-2 #5 shows a low recovery yield (76 % ±10 % – Table 3), while significant and opposite deviations in isotope ratios are observed for RGM-1 #1, #2, BIR-1 and BHVO-2 #4 and #5, which exhibit recovery yields of 95–100 % (±10 % – Table 3). These variations may result from small Nd loss either before or after Nd collection during purification using the LN resin. Although no clear correlation with the measured yield is observed (see Fig. S2) we suggest that samples with <90 % recovery are more likely to present NFS-like isotopic variations. By quantifying Nd content in all LREE, Nd and HREE fractions during the

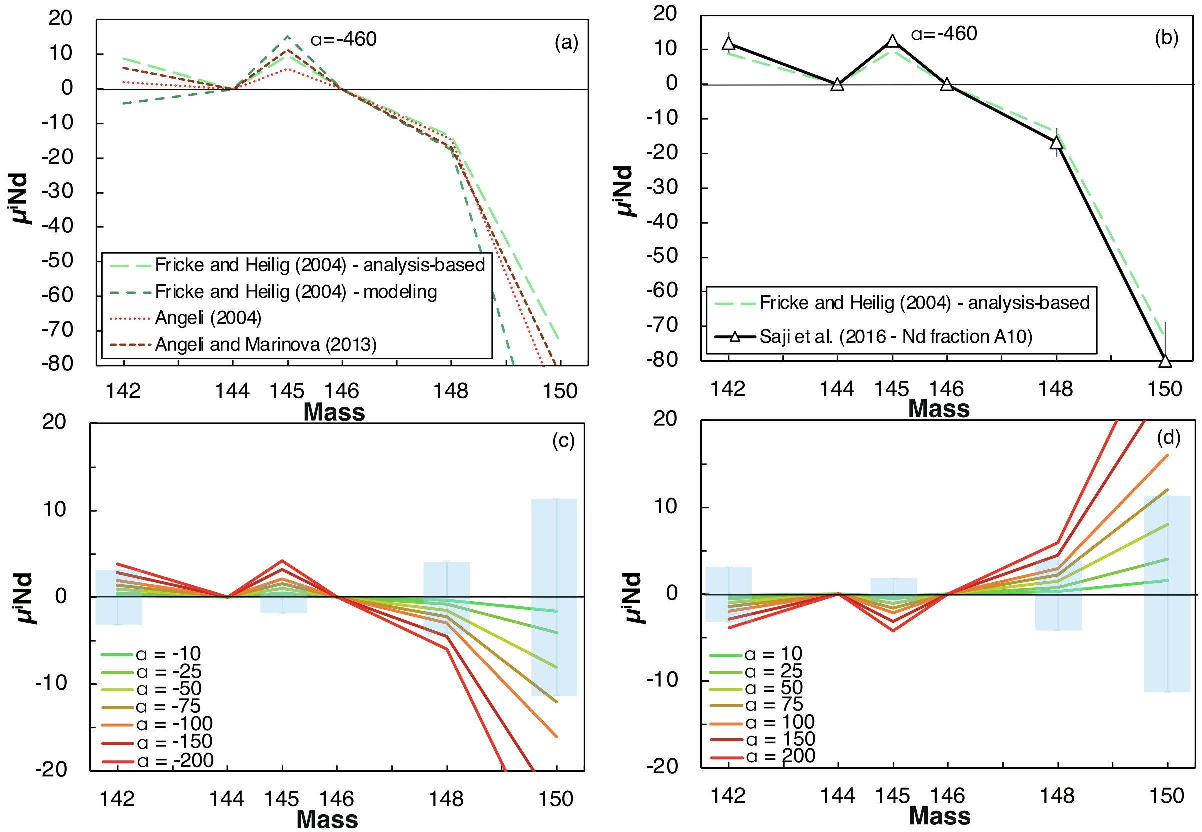

Fig. 10. Theoretical and measured Nd isotope spectra illustrating the effects of the Nuclear Field Shift (NFS) on Nd isotopes. (a) Theoretical NFS-induced Nd isotope spectra calculated using the equations of Fujii et al. (2006, 2009):

$$\mu iNd = \left[\left(\langle r^2\rangle_{iNd} - \langle r^2\rangle_{144Nd}\right) - \frac{m_{146Nd}\times(m_{iNd}-m_{144Nd})}{m_{iNd}\times(m_{146Nd}-m_{144Nd})}\times\left(\langle r^2\rangle_{146Nd}-\langle r^2\rangle_{144Nd}\right)\right]\times\alpha.$$

where $\langle r^2\rangle_i$ is the mean-squared nuclear charge radius of isotope i, m_i is the atomic mass of that isotope and α is the scaling factor defining the intensity of the effect. $\langle r^2\rangle$ from Fricke and Heilig (2004), Angeli, 2004 and Angeli and Marinova (2013), atomic mass from Wang et al. (2012) and $\alpha = -460$. The isotope ratios are expressed in the μ-notation as deviations from the terrestrial reference composition, in ppm. (b) Nd isotope spectra measured in fraction A10 of a sequential elution of Nd as reported in Saji et al. (2016) and compared to the spectra calculated with $\langle r^2\rangle_i$ from Fricke and Heilig (2004) and $\alpha = -460$. (c) and (d) Theoretical NFS-induced Nd isotope spectra modelled using $\langle r^2\rangle$ from Fricke and Heilig (2004 – analysis-based values) for positive and negative α values.

purification using the LN resin, we found that BCR-2 #3–4 and AGV-2 have lost only a few percent of Nd in the HREE-LREE fractions and showed no abnormal isotopic variations whereas BHVO-2 #4–5 had lost ~10 % of Nd in the HREE fraction and showed small positive μ^{148}Nd and μ^{150}Nd. Because even small NFS effects can affect the interpretation of μ^{142}Nd in geochemical and cosmochemical studies, achieving high recovery yields (>90 %) and properly measuring $\mu^{145,148,150}$Nd in terrestrial samples is the most efficient way of improving the reliability of μ^{142}Nd data.

Finally, in Fig. 11g,h, we show how all measurements of JNdi-1 and AMES Rennes Nd compare when looking at deviations relative to a reference value for each isotopic ratio (here taken as JNdi-1 mean for each isotopic ratio). Both standards have similar patterns and undistinguishable compositions for all ^{142,145,148,150}Nd/^{144}Nd ratios (see Figs. 3 and 11g,h). This contrasts with the anomalies reported for the AMES Nd standard by Saji et al. (2016) who suggested that its isotopic composition may have been fractionated during its commercial purification. Here, we suggest that the differences they observe might instead result from their acquisition method on a MC-ICP-MS using JNdi-1 as reference and ^{148}Nd/^{144}Nd as normalization ratio. Indeed, we demonstrated above that the JNdi-1 standard contains traces of Sm that interferes on both masses of the ^{148}Nd/^{144}Nd ratio rather than only one for ^{146}Nd/^{144}Nd. This could amplify corrections for all Nd isotope ratios. We finally conclude that both standards can be used as terrestrial reference as long as Sm interferences are corrected for.

5. Conclusion

The 5-line multi-dynamic method reported in this study for measuring Nd isotopes by TIMS provides unprecedented analytical precision on all Nd isotope ratios. It takes advantage of 14 out of the 16 detectors of the Nu TIMS to provide three dynamic ratios for all Nd isotopes, significantly reducing the bias caused by cup efficiency differences. Optimised emission conditions (high purity zone refined 99.999 % Re filaments, efficient heating procedure and instrumental tuning and excellent vacuum in the source and in the fly tube during the measurement – $\sim 1 \times 10^{-8}$ and $\sim 2 \times 10^{-9}$ mbar, respectively) enable routine 18-h analyses and improved counting statistics, reducing the internal error to less than 2 ppm. This, together with rigorous offline data reduction, results in exceptional long-term precision and accuracy for all Nd isotope ratios. The long-term reproducibility on ^{142}Nd/^{144}Nd is about 3 ppm for both Ames Rennes Nd and JNdi-1 standards over a

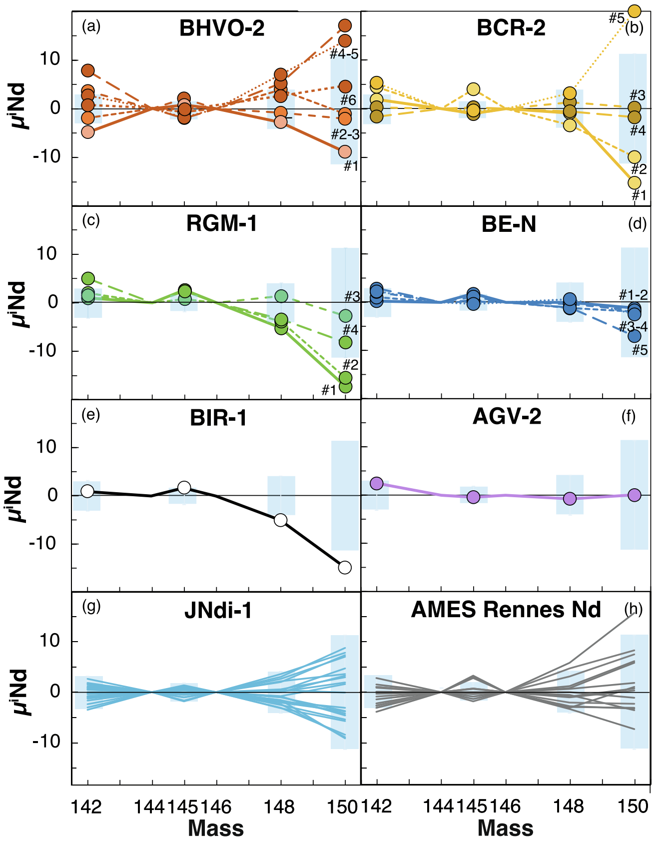

Fig. 11. Neodymium isotope spectra of rock reference materials (a-f), JNdi-1 (g) and AMES Rennes Nd (h) obtained during the course of this study. All data are reported in the μ-notation relative to the average Nd isotope ratios measured for JNdi-1 standard during session 2, whose external error on Nd isotope ratios is represented as blue shaded areas. (For interpretation of the references to colour in this figure legend, the reader is referred to the web version of this article.)

period of 3 years. Reproducibility for the other isotopic ratios is also improved at <6 ppm for ^{143}Nd/^{144}Nd, <3 for ^{145}Nd/^{144}Nd, <6 for ^{148}Nd/^{144}Nd and <13 for ^{150}Nd/^{144}Nd. Both materials have identical Nd isotope ratios except for their ^{143}Nd/^{144}Nd. However, we detect the presence of traces of Sm in JNdi-1, with an impact on the ^{148}Nd/^{144}Nd and ^{150}Nd/^{144}Nd ratios, requiring a Sm interference correction without noticeable effect on the ^{142}Nd/^{144}Nd ratio.

With such high-precision measurements, we are now able to detect minute changes of the ^{142}Nd/^{144}Nd ratios in natural samples, opening up new perspectives in geochemistry for the study of early differentiation events. Isotopic variations due to effects other than radioactive decay can also be better identified; this is particularly the case of NFS effects and their impact on μ^{142}Nd values. Anomalous variations of $^{145, 148, 150}$Nd/^{144}Nd ratios can be used as diagnosis and biased μ^{142}Nd analyses can be eliminated when working on terrestrial samples.

When working on meteorites, acquisition of high-precision data for all Nd isotope ratios should help deciphering nucleosynthetic processes occurring during Solar System formation and evolution, distinguishing the potential building blocks of planets and refining the chronology of Earth, Mars and meteorites parent bodies.

CRediT authorship contribution statement

C. Israel: Writing – review & editing, Writing – original draft, Validation, Methodology, Investigation, Formal analysis, Data curation, Conceptualization. **C. Chauvel:** Writing – review & editing, Writing – original draft, Validation, Supervision, Resources, Project administration, Methodology, Investigation, Funding acquisition, Conceptualization. **T.-H. Luu:** Writing – review & editing, Methodology, Formal analysis, Conceptualization. **E.C. Inglis:** Writing – review & editing, Formal analysis. **D. Roberts:** Writing – review & editing, Software, Methodology.

Declaration of competing interest

The authors declare no financial competing interests.

Acknowledgments

This work was financially supported by the ERC advanced grant SHRED awarded to CC (grant agreement n°833632). Part of this work was supported by IPGP multidisciplinary program PARI, by the Region Ile-de-France SESAME Grants no. 12015908 and EX047016 and by the IdEx Université de Paris grant ANR-18-IDEX0001. We thank the editor Sonja Aulbach and two anonymous reviewers whose comments contributed to significant improvements of the manuscript.

Appendix A. Supplementary data

Supplementary data to this article can be found online at https://doi.org/10.1016/j.chemgeo.2025.122686.

Data availability

Data will be made available on request.

References

Ali, A., Srinivasan, G., 2011. Precise thermal ionization mass spectrometric measurements of 142Nd/144Nd and 143Nd/144Nd isotopic ratios of Nd separated from geological standards by chromatographic methods. Int. J. Mass Spectrom. 299, 27–34. https://doi.org/10.1016/j.ijms.2010.09.014.

Andreasen, R., Sharma, M., 2009. Fractionation and mixing in a thermal ionization mass spectrometer source: implications and limitations for high-precision Nd isotope analyses. Int. J. Mass Spectrom. 285, 49–57. https://doi.org/10.1016/j.ijms.2009.04.004.

Angeli, I., 2004. A consistent set of nuclear rms charge radii: properties of the radius surface R(N,Z). At. Data Nucl. Data Tables 87, 185–206. https://doi.org/10.1016/j.adt.2004.04.002.

Angeli, I., Marinova, K.P., 2013. Table of experimental nuclear ground state charge radii: An update. At. Data Nucl. Data Tables 99, 69–95. https://doi.org/10.1016/j.adt.2011.12.006.

Bigeleisen, J., 1996. Nuclear size and shape effects in chemical reactions. Isotope chemistry of the heavy elements. J. Am. Chem. Soc. 118, 3676–3680. https://doi.org/10.1021/ja954076k.

Bouvier, A., Vervoort, J.D., Patchett, P.J., 2008. The Lu-Hf and Sm-Nd isotopic composition of CHUR: Constraints from unequilibrated chondrites and implications for the bulk composition of terrestrial planets. Earth Planet. Sci. Let. 273, 48–57. https://doi.org/10.1016/j.epsl.2008.06.010.

Boyet, M., Carlson, R.W., 2005. 142Nd evidence for early (> 4.53 Ga) global differentiation of the silicate Earth. Science 309, 576–581. https://doi.org/10.1126/science.1113634.

Burkhardt, C., Borg, L.E., Brennecka, G.A., Shollenberger, Q.R., Dauphas, N., Kleine, T., 2016. A nucleosynthetic origin for the Earth's anomalous 142Nd composition. Nature 537, 394–398. https://doi.org/10.1038/nature18956.

Caro, G., Bourdon, B., Birck, J.-L., Moorbath, S., 2006. High-precision 142Nd/144Nd measurements in terrestrial rocks: constraints on the early differentiation of the Earth's mantle. Geochim. Cosmochim. Acta 70, 164–191. https://doi.org/10.1016/j.gca.2005.08.015.

Chauvel, C., Bureau, S., Poggi, C., 2011. Comprehensive chemical and isotopic analyses of basalt and sediment reference materials. Geostand. Geoanal. Res. 35 (1), 125–143. https://doi.org/10.1111/j.1751-908X.2010.00086.x.

Cook, D.L., Schönbächler, M., 2016. High-precision measurement of W isotopes in Fe–Ni alloy and the effects from the nuclear field shift. J. Anal. At. Spectrom. 31, 1400–1405. https://doi.org/10.1039/C6JA00015K.

Di, Y., Krestianinov, E., Zink, S., Amelin, Y., 2021. High-precision multidynamic Sr isotope analysis using thermal ionization mass spectrometer (TIMS) with correction of fractionation drift. Chem. Geol. 582, 120411. https://doi.org/10.1016/j.chemgeo.2021.120411.

Fang, L., Frossard, P., Boyet, M., Bouvier, A., Barrat, J.-A., Chaussidon, M., Moynier, F., 2022. Half-life and initial Solar System abundance of 146Sm determined from the oldest andesitic meteorite. Proc. Natl. Acad. Sci. 119, e2120933119. https://doi.org/10.1073/pnas.2120933119.

Fourny, A., Weis, D., Scoates, J.S., 2016. Comprehensive Pb-Sr-Nd-Hf isotopic, trace element, and mineralogical characterization of mafic to ultramafic rock reference materials. Geochem. Geophys. Geosyst. 17, 739–773. https://doi.org/10.1002/2015GC006181.

Fricke, G., Heilig, K., 2004. 60-Nd Neodymium. Nucl. Charge Radii 1–10.

Frossard, P., Israel, C., Bouvier, A., Boyet, M., 2022. Earth's composition was modified by collisional erosion. Science 377, 1529–1532. https://doi.org/10.1126/science.abq7351.

Fujii, T., Moynier, F., Albarede, F., 2006. Nuclear field vs. nucleosynthetic effects as cause of isotopic anomalies in the early Solar System. Earth Planet. Sci. Lett. 247, 1–9. https://doi.org/10.1016/j.epsl.2006.04.034.

Fujii, T., Moynier, F., Albarède, F., 2009. The nuclear field shift effect in chemical exchange reactions. Chem. Geol. 267, 139–156. https://doi.org/10.1016/j.chemgeo.2009.06.015.

Fukai, R., Yokoyama, T., 2019. Assessment of the secondary instrumental fractionation in TIMS: Implication for high-precision Nd isotope analysis of geological samples. Geochem. J. 53, 333–337. https://doi.org/10.2343/geochemj.2.0569.

Fukai, R., Yokoyama, T., Kagami, S., 2017. Evaluation of the long-term fluctuation in isotope ratios measured by TIMS with the static, dynamic, and multistatic methods: A case study for Nd isotope measurements. Int. J. Mass Spectrom. 414, 1–7. https://doi.org/10.1016/j.ijms.2016.12.016.

Gannoun, A., Boyet, M., Rizo, H., El Goresy, A., 2011. 146Sm-142Nd systematics measured in enstatite chondrites reveals a heterogeneous distribution of 142Nd in the solar nebula. Proc. Natl. Acad. Sci. 108, 7693–7697. https://doi.org/10.1073/pnas.1017332108.

Garçon, M., Boyet, M., Carlson, R.W., Horan, M.F., Auclair, D., Mock, T.D., 2018. Factors influencing the precision and accuracy of Nd isotope measurements by thermal ionization mass spectrometry. Chem. Geol. 476, 493–514. https://doi.org/10.1016/j.chemgeo.2017.12.003.

Gautam, I., Ray, J.S., Bhutani, R., Balakrishnan, S., Dash, J.K., 2017. Role of fractionation correction in accurate determination of 142Nd/144Nd by TIMS: a case study of 1.48 Ga alkaline rocks from Khariar, India. Chem. Geol. 466, 479–490. https://doi.org/10.1016/j.chemgeo.2017.06.036.

Harper Jr., C.L., Jacobsen, S.B., 1992. Evidence from coupled 147Sm–143Nd and 146Sm–142Nd systematics for very early (4.5-Gyr) differentiation of the Earth's mantle. Nature 360, 728. https://doi.org/10.1038/360728a0.

Hasenstab-Dübeler, E., Tusch, J., Hoffmann, J.E., Fischer-Gödde, M., Szilas, K., Münker, C., 2022. Temporal evolution of 142Nd signatures in SW Greenland from high precision MC-ICP-MS measurements. Chem. Geol. 614, 121141. https://doi.org/10.1016/j.chemgeo.2022.121141.

Horan, M.F., Carlson, R.W., Walker, R.J., Jackson, M., Garçon, M., Norman, M., 2018. Tracking Hadean processes in modern basalts with 142-Neodymium. Earth Planet. Sci. Lett. 484, 184–191. https://doi.org/10.1016/j.epsl.2017.12.017.

Hyung, E., Jacobsen, S.B., 2020. The 142Nd/144Nd variations in mantle-derived rocks provide constraints on the stirring rate of the mantle from the Hadean to the present. Proc. Natl. Acad. Sci. 117, 14738–14744. https://doi.org/10.1073/pnas.2006950117.

Hyung, E., Tissot, F.L.H., 2021. Routine high-precision Nd isotope analyses: an optimized chromatographic purification scheme. J. Anal. At. Spectrom. 36, 1946–1959. https://doi.org/10.1039/D1JA00169H.

Jacobsen, S.B., Wasserburg, G.J., 1980. Sm-Nd isotopic evolution of chondrites. Earth Planet. Sci. Lett. 50, 139–155. https://doi.org/10.1016/0012-821X(80)90125-9.

Le Fèvre, B., Pin, C., 2005. A straightforward separation scheme for concomitant Lu–Hf and Sm–Nd isotope ratio and isotope dilution analysis. Anal. Chim. Acta 543, 209–221. https://doi.org/10.1016/j.aca.2005.04.044.

Luu, T.-H., Gutiérrez, P., Inglis, E.C., Roberts, D., Chauvel, C., 2022. High-precision Sr and Nd isotope measurements using a dynamic zoom lens-equipped thermal ionisation mass spectrometer. Chem. Geol. 611, 121078. https://doi.org/10.1016/j.chemgeo.2022.121078.

Luu, T.-H., Hin, R.C., Coath, C.D., Elliott, T., 2019. Bulk chondrite variability in mass independent magnesium isotope compositions – Implications for initial solar system ^{26}Al/^{27}Al and the timing of terrestrial accretion. Earth Planet. Sci. Lett. 522, 166–175. https://doi.org/10.1016/j.epsl.2019.06.033.

Nyquist, L., Harper, C., Wiesmann, H., Bansal, B., Shih, C.-Y., 1991. 142Nd/144Nd in SNCs and lunar samples: implications for early differentiation of a heterogeneous Martian (?) mantle. Meteoritics 26, 381.

O'Neil, J., Carlson, R.W., Francis, D., Stevenson, R.K., 2008. Neodymium-142 evidence for hadean mafic crust. Science 321, 1828–1831. https://doi.org/10.1126/science.1161925.

O'Neil, J., Francis, D., Carlson, R.W., 2011. Implications of the Nuvvuagittuq Greenstone Belt for the Formation of Earth's Early Crust. J. Petrol. 52, 985–1009. https://doi.org/10.1093/petrology/egr014.

O'Neil, J., Rizo, H., Reimink, J., Garçon, M., Carlson, R.W., 2024. Earth's Earliest crust. Elements 20, 168–173. https://doi.org/10.2138/gselements.20.3.168.

Patchett, P.J., Ruiz, J., 1987. Nd isotopic ages of crust formation and metamorphism in the Precambrian of eastern and southern Mexico. Contrib. Mineral. Petrol. 96, 523–528. https://doi.org/10.1007/BF01166697.

Peters, B.J., Carlson, R.W., Day, J.M.D., Horan, M.F., 2018. Hadean silicate differentiation preserved by anomalous 142Nd/144Nd ratios in the Réunion hotspot source. Nature 555, 89–93. https://doi.org/10.1038/nature25754.

Peters, B.J., Mundl Petermeier, A., Carlson, R.W., Walker, R.J., Day, J.M.D., 2021. Combined lithophile-siderophile isotopic constraints on hadean processes preserved in ocean island basalt sources. Geochem. Geophys. Geosyst. 22. https://doi.org/10.1029/2020GC009479.

Peters, D., Rizo, H., O'Neil, J., Hamelin, C., Shirey, S.B., 2024. Comparative 142Nd and 182W study of MORBs and the 4.5 Gyr evolution of the upper mantle. Geochem. Perspect. Lett. 29, 51–56. https://doi.org/10.7185/geochemlet.2412.

Pin, C., Gannoun, A., 2019a. A triple tandem columns extraction chromatography method for isolation of highly purified neodymium prior to 143 Nd/144 Nd and 142 Nd/144 Nd isotope ratios determinations. J. Anal. At. Spectrom. https://doi.org/10.1039/c8ja00360b.

Pin, C., Gannoun, A., 2019b. Miniaturized, rapid separation of neodymium from ultramafic and chondritic samples prior to high precision measurements of 142,143 Nd/ 144 Nd isotope ratios by TIMS. J. Anal. At. Spectrom. 34, 2136–2146. https://doi.org/10.1039/C9JA00272C.

Rizo, H., Boyet, M., Blichert-Toft, J., Rosing, M., 2011. Combined Nd and Hf isotope evidence for deep-seated source of Isua lavas. Earth Planet. Sci. Lett. 312, 267–279. https://doi.org/10.1016/j.epsl.2011.10.014.

Roth, A.S.G., Bourdon, B., Mojzsis, S.J., Touboul, M., Sprung, P., Guitreau, M., Blichert-Toft, J., 2013. Inherited 142Nd anomalies in Eoarchean protoliths. Earth Planet. Sci. Lett. 361, 50–57. https://doi.org/10.1016/j.epsl.2012.11.023.

Roth, A.S.G., Scherer, E.E., Maden, C., Mezger, K., Bourdon, B., 2014. Revisiting the 142Nd deficits in the 1.48 Ga Khariar alkaline rocks. Chem. Geol. 386, 238–248. https://doi.org/10.1016/j.chemgeo.2014.06.022.

Saji, N.S., Wielandt, D., Paton, C., Bizzarro, M., 2016. Ultra-high-precision Nd-isotope measurements of geological materials by MC-ICPMS. J. Anal. At. Spectrom. 31, 1490–1504. https://doi.org/10.1039/C6JA00064A.

Thirlwall, M., 1991. Long-term reproducibility of multicollector Sr and Nd isotope ratio analysis. Chem. Geol. Isot. Geosci. Sect. 94, 85–104. https://doi.org/10.1016/0168-9622(91)90002-E.

Wang, M., Audi, G., Wapstra, A., Kondev, F., MacCormick, M., Xu, X., Pfeiffer, B., 2012. The Ame2012 atomic mass evaluation. Chin. Phys. C 36, 1603. https://doi.org/10.1088/1674-1137/36/12/003.

Wasserburg, G., Jacobsen, S., DePaolo, D., McCulloch, M., Wen, T., 1981. Precise determination of SmNd ratios, Sm and Nd isotopic abundances in standard solutions. Geochim. Cosmochim. Acta 45, 2311–2323.

Weis, D., Kieffer, B., Maerschalk, C., Barling, J., De Jong, J., Williams, G.A., Hanano, D., Pretorius, W., Mattielli, N., Scoates, J.S., 2006. High-precision isotopic characterization of USGS reference materials by TIMS and MC-ICP-MS. Geochem. Geophys. Geosyst. 7, Q08006. https://doi.org/10.1029/2006GC001283.

Weis, D., Harpp, K.S., Harrison, L.N., Boyet, M., Chauvel, C., Farnetani, C.G., Finlayson, V.A., Lee, K.K.M., Parai, R., Shahar, A., Williamson, N.M.B., 2023. Earth's mantle composition revealed by mantle plumes. Nat. Rev. Earth Environ. 4, 604–625. https://doi.org/10.1038/s43017-023-00467-0.

Yang, S., Liu, Y., 2016. Nuclear field shift effects on stable isotope fractionation: a review. Acta Geochim. 35, 227–239. https://doi.org/10.1007/s11631-016-0109-3.

Zhang, W., Hu, Z., 2020. Estimation of isotopic reference values for pure materials and geological reference materials. At. Spectrosc. 41, 93–102. https://doi.org/10.46770/AS.2020.03.001.

Zheng, W., Hintelmann, H., 2010. Nuclear field shift effect in isotope fractionation of mercury during abiotic reduction in the absence of light. J. Phys. Chem. A 114, 4238–4245. https://doi.org/10.1021/jp910353y.